remote sensing

MDPI

Article

Remote Sensing to Study Mangrove Fragmentation and Its Impacts on Leaf Area Index and Gross Primary Productivity in the South of Peninsular Malaysia

Kasturi Devi Kanniah [1,2,*], Chuen Siang Kang [1], Sahadev Sharma [3] and A. Aldrie Amir [4]

[1] Faculty of Built Environment and Surveying, Universiti Teknologi Malaysia, UTM Johor Bahru 81310, Johor, Malaysia; cskang@utm.my
[2] Centre for Environmental Sustainability and Water Security (IPASA), Research Institute for Sustainable Environment (RISE), Universiti Teknologi Malaysia, UTM Johor Bahru 81310, Johor, Malaysia
[3] Institute of Ocean and Earth Sciences (IOES), University of Malaya, Kuala Lumpur 50603, Wilayah Persekutuan, Malaysia; ssharma@um.edu.my
[4] Institute for Environment and Development (LESTARI), Universiti Kebangsaan Malaysia, Bangi 43600, Selangor, Malaysia; aldrie@ukm.edu.my
* Correspondence: kasturi@utm.my

Abstract: Mangrove is classified as an important ecosystem along the shorelines of tropical and subtropical landmasses, which are being degraded at an alarming rate despite numerous international treaties having been agreed. Iskandar Malaysia (IM) is a fast-growing economic region in southern Peninsular Malaysia, where three Ramsar Sites are located. Since the beginning of the 21st century (2000–2019), a total loss of 2907.29 ha of mangrove area has been estimated based on medium-high resolution remote sensing data. This corresponds to an annual loss rate of 1.12%, which is higher than the world mangrove depletion rate. The causes of mangrove loss were identified as land conversion to urban, plantations, and aquaculture activities, where large mangrove areas were shattered into many smaller patches. Fragmentation analysis over the mangrove area shows a reduction in the mean patch size (from 105 ha to 27 ha) and an increase in the number of mangrove patches (130 to 402), edge, and shape complexity, where smaller and isolated mangrove patches were found to be related to the rapid development of IM region. The Moderate Resolution Imaging Spectro-radiometer (MODIS) Leaf Area Index (LAI) and Gross Primary Productivity (GPP) products were used to inspect the impact of fragmentation on the mangrove ecosystem process. The mean LAI and GPP of mangrove areas that had not undergone any land cover changes over the years showed an increase from 3.03 to 3.55 (LAI) and 5.81 g C m^{-2} to 6.73 g C m^{-2} (GPP), highlighting the ability of the mangrove forest to assimilate CO_2 when it is not disturbed. Similarly, GPP also increased over the gained areas (from 1.88 g C m^{-2} to 2.78 g C m^{-2}). Meanwhile, areas that lost mangroves, but replaced them with oil palm, had decreased mean LAI from 2.99 to 2.62. In fragmented mangrove patches an increase in GPP was recorded, and this could be due to the smaller patches (<9 ha) and their edge effects where abundance of solar radiation along the edges of the patches may increase productivity. The impact on GPP due to fragmentation is found to rely on the type of land transformation and patch characteristics (size, edge, and shape complexity). The preservation of mangrove forests in a rapidly developing region such as IM is vital to ensure ecosystem, ecology, environment, and biodiversity conservation, in addition to providing economical revenue and supporting human activities.

Keywords: mangrove; coastal region; remote sensing; fragmentation; productivity; land cover change

Citation: Kanniah, K.D.; Kang, C.S.; Sharma, S.; Amir, A.A. Remote Sensing to Study Mangrove Fragmentation and Its Impacts on Leaf Area Index and Gross Primary Productivity in the South of Peninsular Malaysia. *Remote Sens.* **2021**, *13*, 1427. https://doi.org/10.3390/rs13081427

Academic Editor: Chandra Giri

Received: 10 March 2021
Accepted: 2 April 2021
Published: 7 April 2021

1. Introduction

Changes in the extent of mangrove cover has resulted in fragmentation that can greatly affect its functions and services to the environment and human kind [1]. Fragmentation of mangrove areas refers to the sub-division of a continuous landscape into smaller units,

which can be characterized based on patch size, edge, and shape modification. Fragmentation analysis and monitoring are important indicators of how mangrove patches influence ecosystem habitats, species diversity, carbon storage capacity, etc. [2]. Bryan–Brown, Connolly, Richards, Adame, Friess, and Brown [1] showed that Southeast Asia (SEA), which has the highest mangrove tree species diversity, is a hotspot for mangrove fragmentation. Among the SEA countries, Malaysia in particular has the highest reduction of mangrove mean patch size, ranked at first place in the nations of the world [1]. Fragmentation could impact habitat health and could cause species extinction, and the report of Ponnampalam et al. [3] showed that Sungai Pulai and Johor Straits in the southern part of Peninsular Malaysia have lost many of their dugong species as a consequence of mangrove loss and fragmentation. Mangroves that provide important economic, social, and ecosystem functions and services [4,5] warrant effective monitoring for appropriate management to avert further loss. The mangrove ecosystem is an essential component of nature-based solutions for climate change mitigation and adaptation [6–8]. While the prevention of deforestation and degradation of mangroves is the most effective strategy for climate change mitigation and adaptation, restoration can reverse the impacts of climate change after 25–30 years [9–11]. Mangroves can protect shorelines against storm surges, cyclones, and tsunami waves. [12,13]. Although recent studies revealed that mangrove loss has been reduced in last decade [14], further and continuous monitoring can help to accelerate the restoration and conservation of mangroves [15].

A review of the literature shows that, in the past decade, although studies on habitat loss is well reported, research on habitat fragmentation has been poorly documented [16]. The limited studies catalogued on habitat fragmentation have focused on nutrient cycling, dung removal, pollination, and seed dispersal [17]. Studies emphasizing the impacts of forest fragmentation on biomass, productivity, predation, parasitism, infection rate, and aquatic functioning account for only 3% of forest fragmentation studies [18]. This gap of information on the impact of fragmentation on mangrove productivity must be addressed and is one of the objectives of the current study. Gross primary production (GPP) of any ecosystem is often used as an indicator of the total amount of CO_2 assimilated by the ecosystem, particularly by the vegetation [19]. Thus, analysis of GPP and its relation to mangrove cover loss and fragmentation can provide useful information pertaining to the dynamics of the mangrove's function to assimilate CO_2. GPP is affected by forest vegetation structure and stand parameters such as the diameter, tree height, canopy area, basal area, leaf area index, and mean tree weight and density [20]. Leaf Area Index (LAI) refers to the total leaf area per unit surface, and this index has been used for assessing the rate of carbon assimilation, primary productivity, and respiration and growth of vegetation, including that of mangroves since the 1990s [21–25] because it is relatively easy to measure in the field and also to derive using remotely sensed data [26]. It can be hypothesized that, due to mangrove forest changes, the LAI of mangroves will be significantly affected, and this will be reflected in the amount of GPP accumulated by mangrove trees. LAI and GPP can therefore be considered as simplified indices to monitor the carbon storage of mangroves. Previous studies have mapped the carbon stock and biomass of mangroves using various remote sensing technology and unmanned aerial vehicle systems [25]. Mangrove biomass assessment and mapping can be done using LAI as an index [27,28].

There have been numerous studies mapping the spatial extent of mangroves and their spatio-temporal changes, and several studies on mangrove ecosystem functions and processes in the past decade [29–33]. However, research focusing on fragmentation and its impact on mangrove biodiversity, biophysical characteristics, and ecosystem processes and functions within the fragmented landscape are scarce. Mangrove fragmentation is assumed to distress ecological processes and ecosystem functioning; thus, establishing a relationship between mangrove cover change, fragmentation, and ecosystem processes will ultimately provide important baseline data for the formation of a stronger policy to protect the remaining mangroves and achieve Malaysia's Sustainable Development Goals, particularly goals 13, on climate action; 14, on life below water; and 15, on life on land.

Remote sensing and Geographic Information System (GIS) are cost- and time-effective technologies that can be used to support large scale mangrove mapping, monitoring its changes [34] and analyzing the landscape's fragmentation [1,2,29]. The launch of the Landsat mission promoted the creation of global and regional mangrove maps at 30 m spatial resolution. These maps can be further improved using freely available satellite images with better spatial resolution, such as that of Sentinel-2. Digital image classification algorithms have been widely developed for obtaining land use and land cover using remotely sensed images. Pixel-based classification involving the unsupervised or supervised method are very common and useful. In the last decade, object-oriented, neural network, decision tree, and machine learning based classification algorithms, with advantages of improved accuracy and reduced computational time, have become more popular. Reviews by Kuenzer et al. [35] and Pham, Xia, Ha, Bui, Le, and Takeuchi [25] concluded that most of the classification algorithms can give overall accuracy above 80%, while, with improvements such as training samples selection, satellite data quality etc., a higher classification accuracy (~90%) can be achieved. Better classification results can improve the mangrove extent mapping and the change detection analysis to accurately detect the gain and loss of mangroves.

This study aims to describe the mangrove loss and fragmentation in the Iskandar Malaysia region over the 2000–2019 period and analyze the loss and fragmentation effects on mangrove LAI and GPP values. More specifically, we intend to (1) document the loss and gain of mangroves over a period of two decades (2000–2019), (2) analyze mangrove fragmentation, and (3) relate and analyze the loss/fragmentation impacts on the LAI and GPP values in order to define the function of mangroves to assimilate CO_2 in relation to mangrove cover changes and fragmentation in the study area. It is hypothesized that a higher loss of mangrove canopy cover and fragmented areas will decrease the LAI and GPP of the ecosystem.

2. Materials and Methods

2.1. Study Area

Malaysia constitutes only 4% of global mangrove cover, but at least 70 true and associated species from 28 families have been identified in the country, and the majority of the mangrove trees are from the *Rhizophoraceae* family [36]. More than half of Malaysian mangroves are distributed in the state of Sabah (60%), 22% in Sarawak, and the remaining 18% are found in Peninsular Malaysia [36]. In Peninsular Malaysia, the majority of mangroves are located along the west coast, and the state of Johor alone holds 30% of the total mangroves (Figure 1). Three of the seven Ramsar Sites in Malaysia, namely Pulau Kukup (647 ha), Tanjung Piai (526 ha), and Sungai Pulai (9126 ha) are located in the Iskandar Malaysia region in Johor (Johor National Parks, https://www.johornationalparks.gov.my/v3/RAMSAR-site/, assessed on 12 December 2020).

Iskandar Malaysia (IM) is a fast-growing national special economic region with a total area of 221,700 ha, located in the southern part of Johor state, Peninsular Malaysia (Figure 1). Specific zones where rapid development has taken place in IM are the Port of Tanjung Pelepas, Tanjung Bin Power Plant, the Port of Pasir Gudang, and the rapid reclamation zone of Forest City, as shown in Figure 1. These activities are mainly caused by population growth that requires more land to be developed for housing establishments, transition to agricultural lands (particularly oil palm), and the building of infrastructure such as ports, dams, and waterfront cities may also lead to fragmentation and impact the carbon sink potential and primary productivity of the mangrove forests in IM. Thus, it is timely to investigate the impact of fragmentation on the primary productivity of the mangrove ecosystem. Although sustainable development policies are employed in the region, the decrease of mangrove forests was found to be at an alarming rate (33%) between 2005 and 2014 [32]. Nevertheless, the replantation and conservation efforts since 2014 may have also increased mangrove coverage; thus, it is important to monitor the changes and analyze their impact on mangrove services.

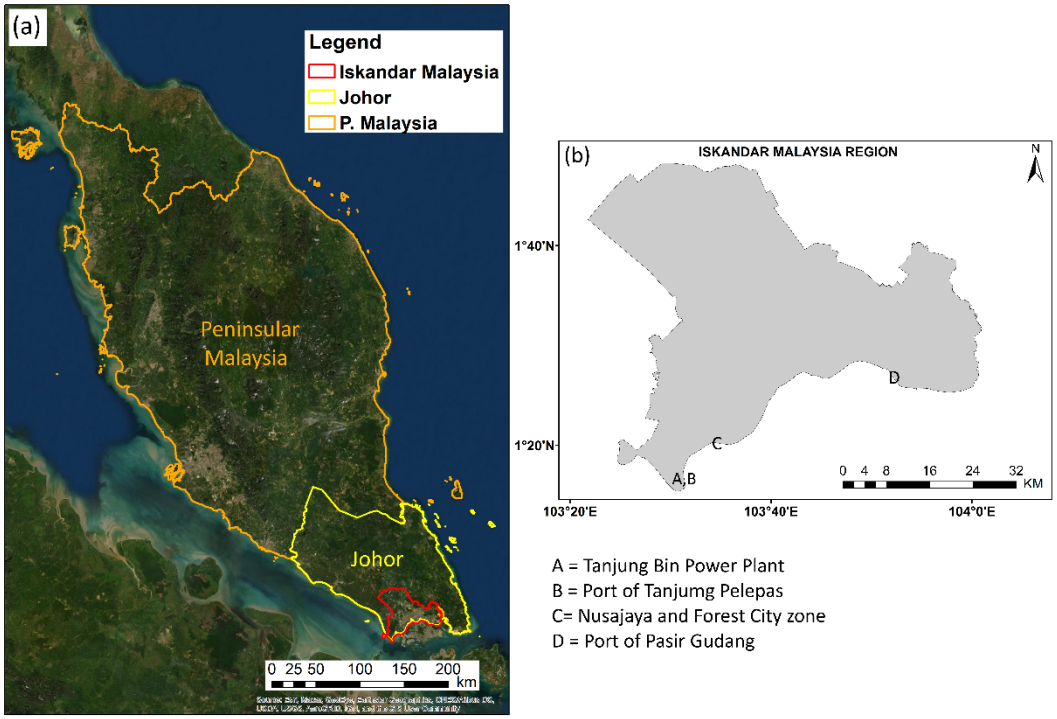

Figure 1. Map of Peninsular Malaysia (**a**) and the region of Iskandar Malaysia (**b**), with four rapidly developing zones (A, B, C, and D) in the region.

2.2. Data and Methodology

The methodology flow-chart (Figure 2) for this study and details on the data processing and the methods to achieve the aim of the study are described in the following sections. This study utilized medium-resolution remote sensing satellite imageries to monitor changes in mangrove cover and fragmentation, covering the years 2000 to 2019. Support Vector Machine (SVM) was selected as the classifier for the image classification process. A patch analysis plugin was implemented for fragmentation analysis based on ArcGIS software. The land cover, LAI, and GPP Products of Moderate Resolution Imaging Spectroradiometer (MODIS) Collection 006 were used to define the impact of loss and fragmentation on mangrove forests in IM. The MODIS Land Cover Product is based on a supervised decision-tree classification method using inputs from other MODIS products, including the land/water mask, nadir bidirectional reflectance distribution function (BRDF)-adjusted reflectance, Enhanced Vegetation Index (EVI), snow cover, land surface temperature, terrain elevation information, etc. [37]. The MODIS LAI product incorporated the MODIS Land Cover Product and MODIS Surface Reflectance Product into the radiative transfer model to derive LAI [38]. The MODIS GPP product is derived by relating the absorbed photosynthetically active radiation (APAR) calculated from LAI with the energy conversion efficiency (ε) [26]. More information of the MODIS products and the method to access these products are described below.

2.2.1. Remote Sensing Data and Pre-Processing

Landsat 7 Enhanced Thematic Mapper Plus (ETM+) Terrain Corrected (L1T), data dated 28 April 2000, was downloaded from the GloVis website (https://glovis.usgs.gov/ (accessed on 15 March 2021)). This data is registered on the Worldwide Reference System-2 (WRS-2), and one tile (Path 125, Row 59) is required to cover the whole Iskandar Malaysia zone. A sentinel-2 Level-1C multispectral image dated June 28, 2019, was chosen to present the latest conditions of the study area because no Landsat image with acceptable cloud cover was available. The image was downloaded from the Copernicus Open Access Hub (https://scihub.copernicus.eu/ (accessed on 15 March 2021)). For both Landsat 7 and

Sentinel-2, only images with less than 20% cloud cover were used. The Semi-Automatic Classification plug-in (SCP) provided in the QGIS software [39] was used to perform the preprocessing of Landsat 7 and the Sentinel-2 images.

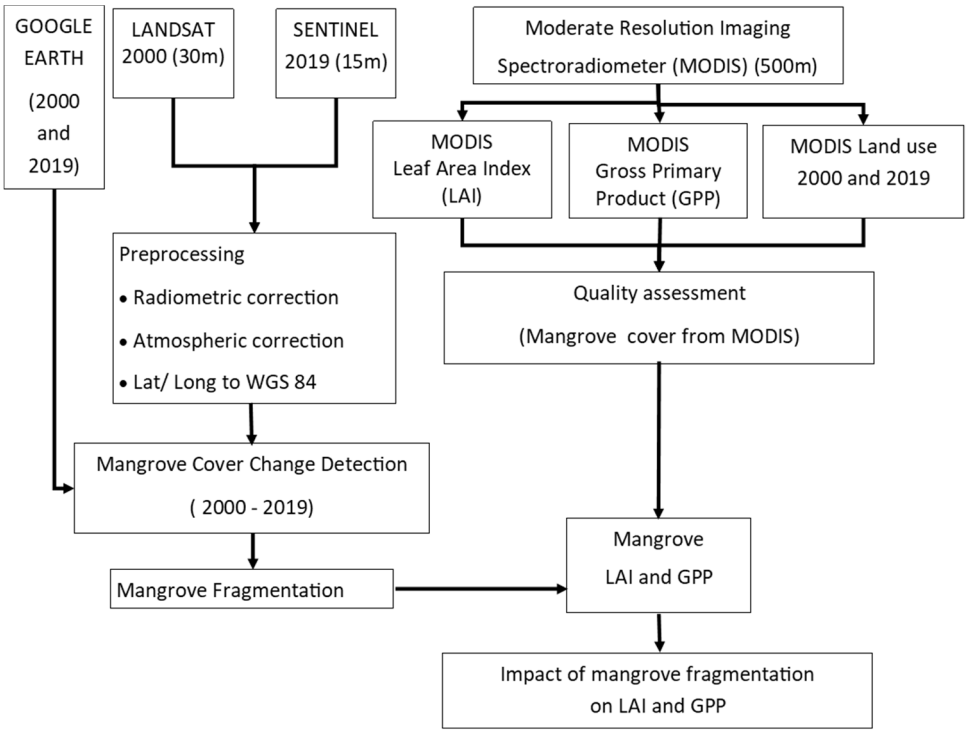

Figure 2. The work-flow chart for image processing, classification and assessment, fragmentation, LAI and GPP analysis.

Preprocessing, including radiometric correction and atmospheric correction based on the Dark Object Subtraction 1 (DOS 1) model and pan-sharpening model, was applied to the Landsat 7 image. The radiometric and atmospheric correction transferred the digital numbers (DN) to radiance then to reflectance. The pan-sharpening function, based on intensity computation, fused the 30 m Landsat multispectral bands (6 bands covering the visible (blue, green, red), near infrared, and shortwave infrared) with the panchromatic band to produce a 15 m spatial resolution reflectance image. The Sentinel-2 image underwent similar preprocessing steps (radiometric and atmospheric correction using DOS 1) based on the SCP. The visible bands (band 2—blue, 3—green, 4—red) and near infrared (band 8) of 10 m spatial resolution were stacked in this case. The output was a 4-band multispectral reflectance image at 10 m spatial resolution. A thresholding method based on the reflectance of the blue band (>0.25 for Landsat 7 and >0.21 for Sentinel-2) was applied to detect and mask out any cloud on the image. Note that, for both Landsat and Sentinel images, only a very low cloud cover was detected over the mangrove areas, which is the main focus of this study.

Three latest MODIS products (Collection 006) at 500 m spatial resolution were downloaded, namely the MOD15A2H (Leaf Area Index, LAI) [38], the MOD17A2H (Gross Primary Production, GPP) [26], and the MCD12Q1 (Land cover type, LC) [37]. Only one tile (H28.V08) is required to cover the whole IM region. Both LAI and GPP are 8-day composite products. Full year products of 2000 and 2019 were downloaded for LAI and GPP, which consisted of 39 tiles for year 2000 (MODIS started to provide data from 18 February 2000) and 46 tiles for year 2019. Meanwhile, the yearly composite (one product per year) LC product for years 2000 and 2019 were downloaded. All the MODIS products are available from the NASA Earthdata website (https://earthdata.nasa.gov/ (accessed on 15 March 2021)). The MODIS Conversion Toolkit (MCTK) was used to process the MODIS products, including re-projection and quality check (QC) assessment. In order to maintain the quality

of the LAI and GPP products, pixels with a QC bit-converted value below 48 were kept and extracted, referring to the MODIS product user guides [26,38,40]. The products were re-projected into WGS 84 projection, and the QC considered the sensor, detectors, and cloud condition issues of the product. For the LC product, we selected the International Geosphere-Biosphere Program (IGBP) layer for this study. According to the IGBP layer, the permanent wetlands (PW) pixels (LC code 11) were identified. The corresponding LAI and GPP values located in the identified PW pixels were extracted with the strict consideration of the QC. The mean and standard deviation of the LAI and GPP at 8-day intervals were computed for further analysis.

2.2.2. Image Classification and Assessment

Support Vector Machine (SVM) classification has been one of the most applied classifiers in recent years. SVM uses the machine learning technique for multispectral and hyperspectral remotely sensed data classification. SVM relies on n-dimensional spectral space to create a hyperplane and identify and separate the classes based on user optimized parameters, including the selection of kernel type and function and the penalty parameter [41]. A total of 7 land use/land cover classes were detected and discriminated from the Landsat and Sentinel images based on the SVM, as follows: terrestrial forest, mangrove forest, oil palm plantation, rubber plantation, urban, water, and others (orchard, shrub, bush, aquaculture farms, etc.). The details of the parameters needed to run the SVM classifier are listed in Table 1. The classification was run based on a total of 140 training data (20 polygons per class with 50–60 pixels per polygon), where different sets of training data were selected during Landsat 7 and Sentinel 2 classification. Figure A1 in the Appendix A shows the training polygons for the Landsat and Sentinel classification. The accuracy assessment of the classified land covers/uses was based on the sample points selected from the Google Earth images as the "ground truth" samples. Google Earth is notably one of the most complete and useful datasets with acknowledged accuracy, and is also freely available for various types of research, including classification and its validation [42–44]. Classification assessment based on the error matrix was performed. The overall accuracy (OA) is the ratio between the correctly classified pixels to the total number of reference pixels. The producer accuracy (PA) is the accuracy of the map from the perspective of the map maker, computed by dividing the correctly classified samples of the class to the sum of the reference samples for the class. The user accuracy (UA) is the accuracy from the point of view of a map user, calculated by dividing the correct classification pixels to the total number of pixels mapped as the class. The kappa coefficient (KC) is a value computed based on the KHAT statistic to measure the agreement and accuracy of the classification. In addition, the Z-statistic has been computed to describe the significance of the classification results. The function of the Z-statistic is to determine if the agreement between the classification map significantly agrees with the reference data [45].

Table 1. Parameters for Support Vector Machine (SVM) classification.

Parameter	Type/Value
Kernel type	Radial Basis Function (RBF)
Gamma in kernel function	1.00
Penalty	100
Pyramid levels	0
Region of Interests (ROI)	140 (20 polygons for each class)

2.2.3. Mangrove Cover Change and Fragmentation

After the accuracy assessment of the 2000 and 2019 classification results, the classified mangrove areas were extracted from the classified map. Because the classification maps are in raster form, we converted the maps into vector polygons using the Raster to Polygon function in the ArcGIS software. Change detection was performed based on the polygons using ArcGIS software to detect the unchanged, gained, and lost mangrove areas in IM

between 2000 and 2019 by superimposing the mangrove cover from 2000 onto the results of 2019.

The Patch Analyst extension in ArcGIS 10.5 was used as the tool for fragmentation analysis. Patch Analyst is based on the FRAGSTATS [46], which can be used for analysis and to provide attributes of the fragmented patches. Several indices were selected in this study to represent the fragmentation of the mangrove area in IM, including Class Area (CA), Total Landscape Area (TLA), Number of Patches (NP), Mean Patch Size (MPS), Total Edge (TE), Edge Density (ED), Mean Shape Index (MSI), Average Weighted MSI (AWMSI), Mean Perimeter Area Ratio (MPAR), and Mean Patch Fractal Dimension (MPFD). The group and details of each index is listed in Table 2. Because mangrove is the focus of the study, the fragmentation analysis was performed for mangrove areas only.

Table 2. List of metrics in the Patch Analyst extension used for fragmentation analysis [46].

Group	Fragmentation Index	Definition
Area	Class Area (CA) Total Landscape Area (TLA)	Sum of areas of all patches of a given class Sum of areas of all patches in the landscape
Patch size	Number of Patches (NP) Mean Patch Size (MPS)	Total number of patches in the class/landscape Average patch size
Edge	Total Edge (TE) Edge Density (ED)	Total perimeter of patches Amount of edge relative to the landscape area
Shape	Mean Shape Index (MSI) Average Weighted MSI (AWMSI) Mean Perimeter Area Ratio (MPAR) Mean Patch Fractal Dimension (MPFD)	Average perimeter-to-area ratio MSI divided by weighted patches area Average of patch perimeter to patch area ratio Average of log-transformed patch perimeter to log-transformed patch area ratio

2.2.4. Mangrove LAI and GPP

LAI and GPP are both useful for studying the coverage, health, and potential of carbon assimilation and storage [47]. Mangrove forests have been proven as the highest carbon stock medium; nevertheless, the role of mangrove forest in carbon assimilation and its processes from local to global scale is less understood. This is due to the difficulties of data collection in the mangrove forests. Plant leaves through the photosynthesis process convert the atmospheric CO_2 into nutrients and biomass to support plant growth. The use of LAI to estimate the ecosystem carbon uptake by linking it with GPP is common [48,49]. Remote sensing products were applied in this study to infer the leaf density and productivity of mangrove areas, aimed at detecting the impact of mangrove changes to the products (LAI and GPP) relevant to carbon stock.

To identify the impact of mangrove loss and fragmentation over years, the MODIS LAI and GPP of the permanent wetlands (PW) (based on MODIS IGBP land cover classification) were extracted. LAI can be used to describe the leaf density and therefore the vegetation condition/health/ photosynthesis rate and light use efficiency of the mangrove trees [33,34]. We chose LAI as the vegetation index because it is often widely applied to high leaf and tree density zones, including mangrove forests [50], and LAI has been proven to have a strong relationship with Normalized Difference Vegetation Index (NDVI) at different spatial resolutions [51,52]. Meanwhile, MODIS GPP is an indication of the amount of CO_2 assimilated by the ecosystem; thus, it can be used to identify carbon gain/loss due to any changes occurring in the ecosystem. Here, we used GPP rather than NPP because (1) GPP has more direct relations to the photosynthesis rate, leaves, and biomass growth, (2) NPP requires the input of respiration (data is very hard to acquire and not available in the study site), and (3) MODIS only distribute the NPP product at an annual timespan, while we aim to compare GPP and LAI at finer temporal scales (8-days). The values of LAI and GPP were extracted and their statistical values were computed to identify if any loss

or gain had occurred in LAI or carbon intake by mangroves (to the selected permanent wetlands pixels).

3. Results

3.1. Classification Accuracy and Mangrove Cover Changes

Using the SVM classifier, seven land use/land cover classes, including forest, oil palm, mangrove, rubber, urban, water, and "others", were classified. The class "others" includes orchard, shrub, bush, farm, and aquaculture. Table 3 reports the accuracy of the classification from the two satellite images, including the producer accuracy (PA), user accuracy (UA), overall accuracy (OA) and the kappa coefficient (KC). The overall accuracy of both images is ~90%, with a KC of 0.85 and 0.88 for the 2000 and 2019 classifications, respectively. Both the Landsat 7 and Sentinel-2A classification results showed a high accuracy of around 90%, which may be because of their finer spatial resolution and multi spectral bands, and is also due to the machine learning technique of SVM. On the other hand, the pan-sharpened Landsat image also maintained high classification accuracy when more bands (more information) were considered during the classification process. Z-statistics were computed for both classification results, where both values were higher than 1.96, indicating that the classification is meaningful and significant and the classification results are better than random classification.

Table 3. Distribution of land use area and the producer accuracy (PA), user accuracy (UA), overall accuracy (OA), and kappa coefficient (KC) for respective class *.

Class	Landsat 7 (2000)		Sentinel-2A (2019)	
	PA (%)	UA (%)	PA (%)	UA (%)
Forest	89.25	92.45	78.22	87.93
Mangrove	97.52	90.64	87.85	99.70
Oil Palm	88.66	78.35	73.02	84.47
Rubber	43.17	78.15	96.40	53.49
Urban	64.56	93.12	95.44	93.88
Water Bodies	98.56	99.57	92.55	98.17
Others	46.32	19.19	91.42	62.67
OA	89.96%		90.51%	
KC	0.85		0.88	
Z-statistic	271.37		109.35	

* The definition of land cover types is given in Table A1.

Because the general land use land cover changes are similar to the previous findings in Kanniah, Sheikhi, Cracknell, Goh, Tan, Ho, and Rasli [32], we omitted the land use maps in this study and focused only on the mangrove cover in the following results and discussions. In this study, we further found an expansion of the urban area, especially at the eastern part of Sungai Pulai, where the new Nusajaya township is located, and in the central part of IM, where the Kulai–Senai township has expanded due to increased population. Rubber conversion to oil palm plantation and urban area is still found (in 2019 image) surrounding the Sultan Iskandar Reservoir in the eastern part of IM, showing similar results to [32] in their 2014 satellite data.

The use of the SVM classifier showed great capability by clearly distinguishing mangroves from forests and water bodies, which often can be easily misclassified. Both the user and producer accuracies are high for mangrove classification in the 2000 and 2019 images (Table 3). From the classification results, the loss of mangrove area is noticeable, particularly where it has been converted to urban area and oil palm plantations. Interestingly, the conversion of mangrove to aquaculture land use (classified as "others") was found at multiple locations, which showed the recent development and expansion of the economically valuable aquaculture activities in the IM region (Table 4 and Figure 4b). The performance of SVM classification in this study supports the accuracy of mangrove loss and

gain detection (Table 4 and Figure 4), as well as clearly identifying fragmented mangrove patches (Table 6).

Table 4. The loss and gain of mangrove areas and their transition to other land use/cover types in IM between 2000 and 2019.

Gain ID.	Places/Location	Transition Type
1	Pulau Kukup	Eroded mangrove
2	Serkat Berkat Village	Oil palm
3	Tanjung Piai	Eroded mangrove
4	Perpat Pasir Village	Oil palm
5	Sungai Boh Village	Urban
6	Pulai River—Custom Administration Building	Urban
7	Forest City Golf Hotel/ Resort	Urban—resort
8	Sri Tulang Residential Project	Urban—residential
9	Bayu Senibong Residential zone	Bare land
10	Changkat Village	Aquaculture
11	Sri Aman Village	Aquaculture
12	Sri Aman Village	Aquaculture
13	Sri Aman Village	Aquaculture
14	Tanjung Langsat	Urban—port expansion
15	Tanjung Langsat	Urban—port expansion
16	Kampung Kong Kong	Aquaculture
17	Kampung Kong Kong	Aquaculture
18	Layang River	Eroded mangrove
19	Tiram River Fishing Village	Aquaculture
20	Tiram River Fishing Village	Aquaculture
21	Tiram River Fishing Village	Aquaculture
Gain ID.	**Places/Location**	**Transition Type**
1	Kong Kong River	Eroded mangrove
2	Kong Kong River	Eroded mangrove
3	Tanjung Langsat Village	Aquaculture
4	Melayu Village	Aquaculture

Based on the classification results, the total mangrove areas in 2000 and 2019 were 13,612.25 ha and 10,704.96 ha, respectively. Figure 3 shows the mangrove areas, their gain, and their loss, and unchanged mangrove areas between 2000 and 2019. The total unchanged mangrove areas over the 19-year period was 8483.44 ha, and the total loss was 5128.80 ha. Despite the loss, some new (2171.38 ha) mangrove areas were detected. This means that a net loss of 2907.29 ha (21.35%) has occurred in IM over the last 19 years. This is equal to a 1.12% annual mangrove loss in the IM region, which is higher than Malaysia's mean depletion rate of 0.41%, based on the estimation of Hamilton and Casey [53]. The southwestern part of the IM, where the Pulau Kukup, Tanjung Piai, and Sungai Pulai mangrove forests (Ramsar sites) are located (Figure 3c), faced significant loss over the study period. On the other hand, at the eastern side of IM, new patches of mangroves were noticed. Figure 4a shows the pinned locations of gain and loss of mangroves over the IM region. Table 4 lists the locations and types of transition from (loss) and to (gain) mangrove area, with Table 5 showing the conditions of some selected loss and gain areas, including when these transitions occurred. During the identification of the gain and loss locations, we also identified around 40 sites in IM that were used for aquaculture activities (Figure 4b).

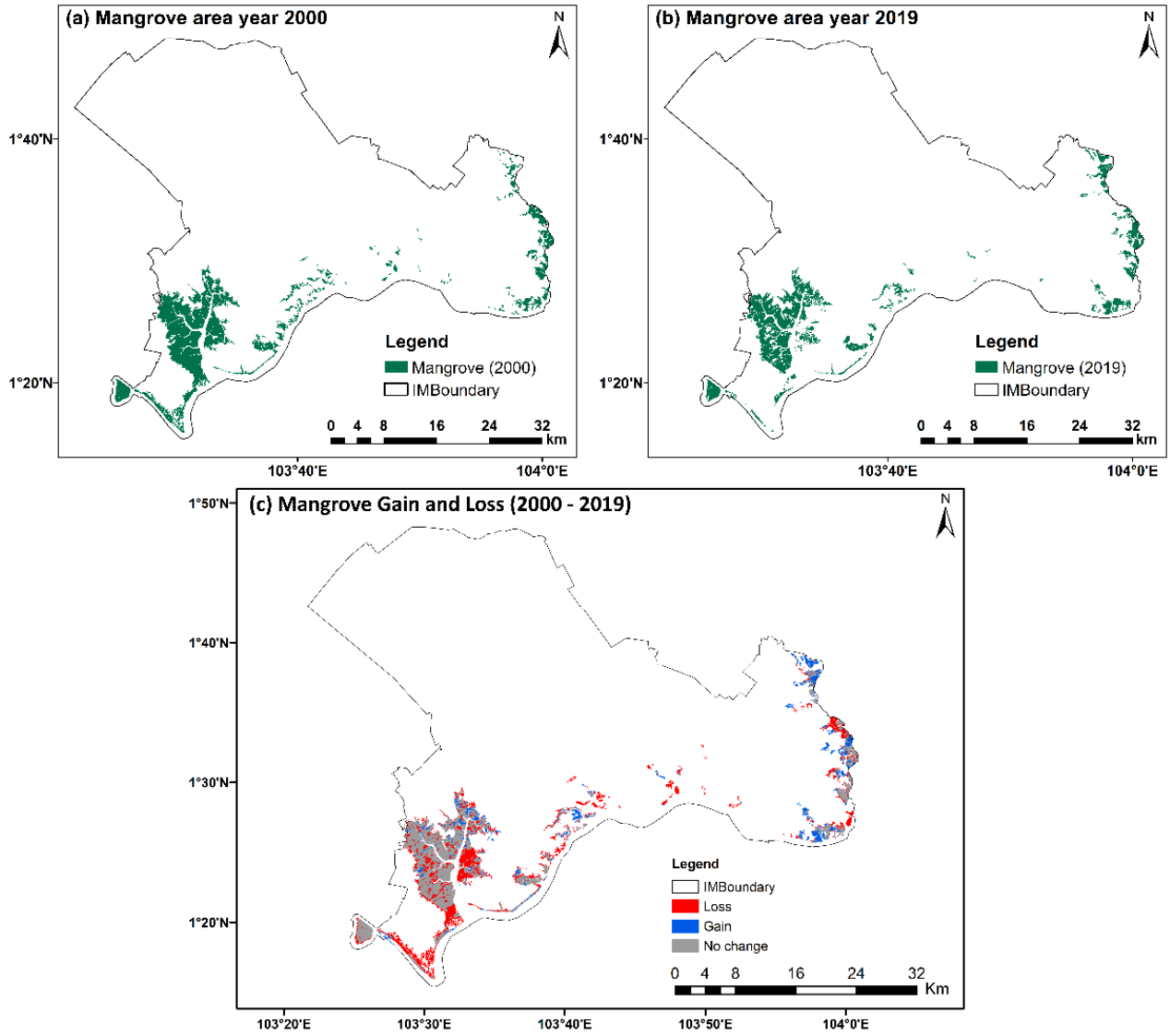

Figure 3. Mangrove area of (**a**) year 2000; (**b**) year 2019; and (**c**) the unchanged, gains, and losses of mangroves between 2000 and 2019.

3.2. Fragmentation Analysis

Fragmentation results in Table 6 show that the IM region underwent significant fragmentation over the two decades of the study period. Since we considered only one class (mangrove) in the fragmentation analysis, the area indices, including class area (CA) and total landscape area (TLA), are the same, which is 13,612 ha and 10,705 ha for years 2000 and 2019, respectively. There was a significant loss of mangrove area (21%) during the study period; thus, the analysis of the remaining fragmentation metrics will also be focused on the influence of the area loss on each metric.

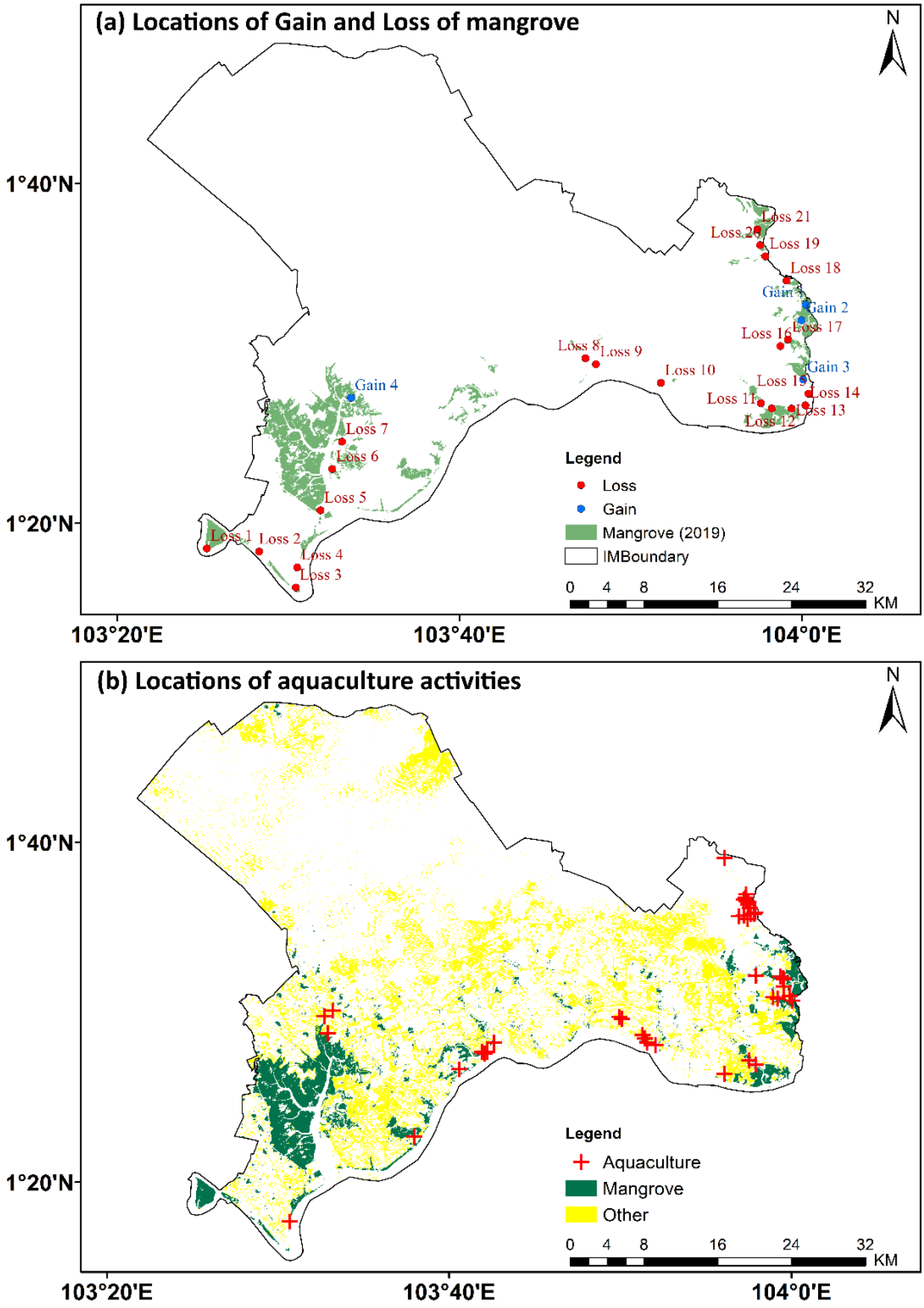

Figure 4. Identification of areas of (**a**) gain and loss and (**b**) aquaculture over Iskandar Malaysia (IM).

Table 5. Selected loss and gain of mangrove areas and their transition conditions. Different years are based on the availability of the Google Earth images. Pins shown on the images correspond to the location of gain and loss in Figure 4a.

Transition Type	ID.	Loss Area		
		Pulau Kukup		
			23 Aug 2006	2 Aug 2019
Eroded mangrove	1	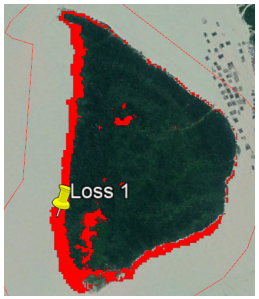		
		Layang River		
			6 Apr 2003	30 June 2017
	18			

Table 5. *Cont.*

Transition Type	ID.	Loss Area		
Urban	5	Sungai Boh Village		
			17 Jan 2008	10 Feb 2018
		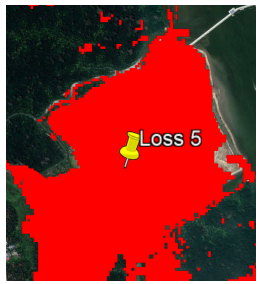		
	6 and 7	Pulai River—Custom Administration Building and Forest City Golf Hotel/Resort		
			July 2006	2 Aug 2019
		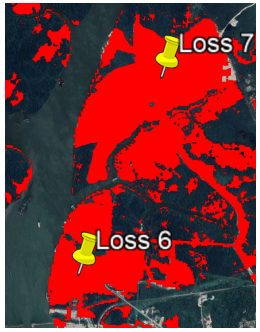	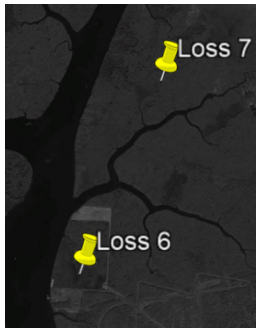	

Table 5. *Cont.*

Transition Type	ID.	Loss Area		
		Sri Aman Village		
	11 and 12		6 Apr 2003	23 Jan 2012
		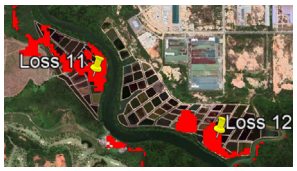		
		Kong Kong Village		
Aquaculture	16 and 17		6 Apr 2003	19 July 2020
		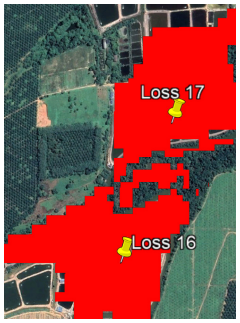		

Table 5. *Cont.*

Transition Type	ID.	Loss Area		
		Gain area		
Eroded mangrove	1 and 2	Kong Kong River		
			6 Apr 2003	30 June 2017
		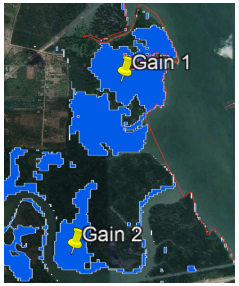		
Aquaculture	3	Tanjung Langsat Village		
			6 April 2003	10 Nov 2019
		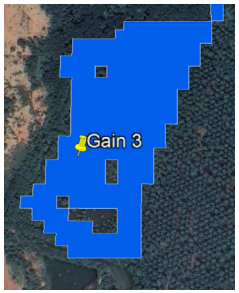		

Table 5. *Cont.*

Transition Type	ID.	Loss Area		
		Gain area		
			Melayu Village	
			17 Jan 2008	2 Aug 2019
	4	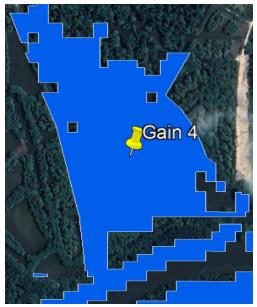		

Table 6. Fragmentation values for the year 2000 and the year 2019.

Index	Unit	Year 2000	Year 2019
Class Area (CA)	ha	13,612	10,705
Total Landscape Area (TLA)	ha	13,612	10,705
Number of Patches (NP)	-	130	402
Mean Patch Size (MPS)	ha	104.71	26.63
Total Edge (TE)	m	1,200,480	1,364,970
Edge Density (ED)	m/ha	88.20	127.509
Mean Shape Index (MSI)	-	2.796	1.962
Average Weighted MSI (AWMSI)	-	8.802	8.761
Mean Perimeter Area Ratio (MPAR)	m/ha	245.95	1685.40
Mean Patch Fractal Dimension (MPFD)	-	1.366	1.444

The patch size index provides information about the Number of Patches (NP) and the Mean Patch Size (MPS). The patch size is one of the fragmentation parameters that has been studied most [17]. Increased NP from 130 to 402 and decreased MPS from 104.71 to 26.63 (reduction of −78.08 ha) between 2000 and 2019 indicates that the mangrove areas in the IM region had been broken down into smaller patches. The changes of minimum patch size (3.08 ha to 0.001 ha) and maximum patch size (6883.01 ha to 4067.96 ha) from years 2000 to 2019 showed a similar trend to the MPS values, indicating that the mangrove areas had been fragmented into smaller patches throughout the entire study area. In a previous study, Bryan–Brown, Connolly, Richards, Adame, Friess, and Brown [1] reported a smaller reduction of mean patch size of −7.2 ha for Malaysia between 2000 and 2012, which infers that the fragmentation in the IM region is significantly more serious than the country's average. The higher MPS could also be due to the more rapid development in IM compared to other cities located near to mangrove forests in other parts of Malaysia. Coincidentally, the largest mangrove patch in the year 2019 (4067.96 ha) was found located in the largest mangrove patch of the year 2000 (6883.01 ha). Analysis of this large mangrove patch showed that it had fragmented into 60 smaller patches (0.001 ha to 4067.96 ha, with a mean of 94.29 ha), with a loss of 1131.63 ha over the study period. This specific patch has been selected for detailed fragmentation analysis on its effect of LAI and GPP in the later part of this manuscript.

Similarly, the Edge indices (TE and ED) also increased from 2000 to 2019, primarily because of the separation of large patches into small patches. Figure A2 in the m shows the fragmentation of mangrove over a selected area within the study area. The increases in TE (from 1200.5 km to 1365 km) and ED (from 88.2 m/ha to 127.5 m/ha) demonstrate that the fragmentation is a result of man-made disturbances rather than natural effects. This can be explained by natural shaped patches normally having fewer edges than man-made urban areas and agriculture boundaries. The values of patch size and edge indices obtained in this study show typical mangrove forest fragmentation over a rapidly developing region, where the disturbance of a large mangrove area into smaller patches occurred due to the transformation of mangroves into urban, agriculture, and aquaculture lands. Generally, the decrease in any forest habitat area or MPS has been shown to create fragments of different sizes (large and small) and isolation among the fragmented patches. Hence, this can result in species extinction and biodiversity loss due to decreased colonization and population size [17,54].

The Shape metrics (MSI, AWMSI, and MPAR) explain the changes of the mangrove areas shape from regular to more complex patches. An MSI of 1 refers to a circular shape, and higher values indicate more irregular shape patterns. The MSI calculated in this study changed from 2.79 in 2000 to 1.96 in 2019, meaning that the complexity of the shape of the patches was reduced. This phenomenon indicates that the mangrove patches change from natural shaped patches (complex in shape) to man-made shape (regular in shape), due to anthropogenic activities [46,55]. The AWMSI refers to the area weighted MSI, which highly depends on the area of patches and the NP. Slightly lower AWMSI was found in 2019 compared to 2000 due to a decrease in the sum of patch area and a large increase of NP.

This indicates that the MSI was divided by a relatively larger value in 2019 than in 2000, meaning that there were more fragmented patches in the region in 2019. MPAR, which considers the mean perimeter-to-area ratio shows an increased value for 2019 compared to 2000. Smaller patches with decreasing areas and relatively longer perimeters are the main reason for the large increase in MPAR. Finally, the MPFD, which has values between 1 (simple shaped) to 2 (complex shaped) have increased between 2019 and 2000, showing that the fragmented patches of mangrove in 2019 were more irregular compared to larger mangrove patches in 2000.

3.3. LAI and GPP Analysis

LAI and GPP values for the MODIS IGBP Permanent Wetlands (PW) pixels were extracted. The classified mangrove and MODIS PW pixels of 2000 and 2019 are shown in Figure 5. There were 559 and 388 MODIS PW pixels (500 m) for years 2000 and 2019, respectively, and most of the MODIS PW pixels are located within the classified mangrove area (68% for the year 2000 and 65% for the year 2019). This means that MODIS PW pixels can be used to extract the LAI and GPP values and to analyze their changes over time due to mangrove area changes. The converted total area of MODIS PW is 13,975 ha for the year 2000 and 9700 ha for the year 2019, which was found to be close to the area based on the classification in this study (13,612.25 ha and 10,704.96 ha, in Section 3.1). Similar to the classification result (Figure 3a,b), most of the disappearance of PW pixels were noticed over the Sungai Pulai and Tanjung Piai area (Figure 5).

The mean and standard deviation of MODIS LAI and GPP at 8-day intervals for 2000 and 2019 are plotted and shown in Figures 6 and 7. Five cases are plotted and discussed namely: (1) mean LAI and mean GPP extracted over all mangrove areas—Figures 6a and 7a, (2) mean LAI and mean GPP extracted over areas where mangrove is unchanged—Figures 6b and 7b, (3) mean LAI and mean GPP extracted over areas where a mangrove gain is detected—Figures 6c and 7c, (4) mean LAI and mean GPP extracted over areas where a mangrove loss is detected—Figures 6d and 7d, and (5) mean LAI and mean GPP extracted over selected fragmented areas—Figures 6e and 7e. Table 7 summarizes the mean and standard deviation values of LAI and GPP for these cases. Note that there are some missing data in these graphs due to unsuccessful retrieval of the MODIS products on certain dates that could be due to cloud cover, failure of detectors, or failure of the main radiative transfer algorithm used to retrieve the LAI/GPP values. The analysis starts from day of year (DOY) 57 because the MODIS LAI and GPP products are only available after February 2000.

Table 7. Mean and standard deviation of LAI and GPP from MODIS products. Values in parentheses refer to the number of pixels involved in each extraction.

	LAI		**GPP (g C m^{-2})**	
	2000	**2019**	**2000**	**2019**
All PW	3.18 ± 1.56 (145)	3.46 ± 2.09 (84)	6.82 ± 15.26 (141)	5.49 ± 15.10 (77)
Unchanged	3.03 ± 1.94 (89)	3.55 ± 1.97 (67)	5.81 ± 14.05 (87)	6.73 ± 16.65 (65)
Gain	2.81 ± 1.79 (24)	3.51 ± 2.20 (16)	1.88 ± 6.75 (25)	2.78 ± 8.88 (16)
Loss	2.99 ± 2.02 (52)	2.62 ± 2.15 (37)	6.38 ± 14.34 (50)	6.88 ± 15.60 (37)
Fragmented	3.11 ± 1.71 (74)	3.41 ± 1.79 (42)	4.65 ± 12.76 (71)	6.37 ± 16.46 (42)

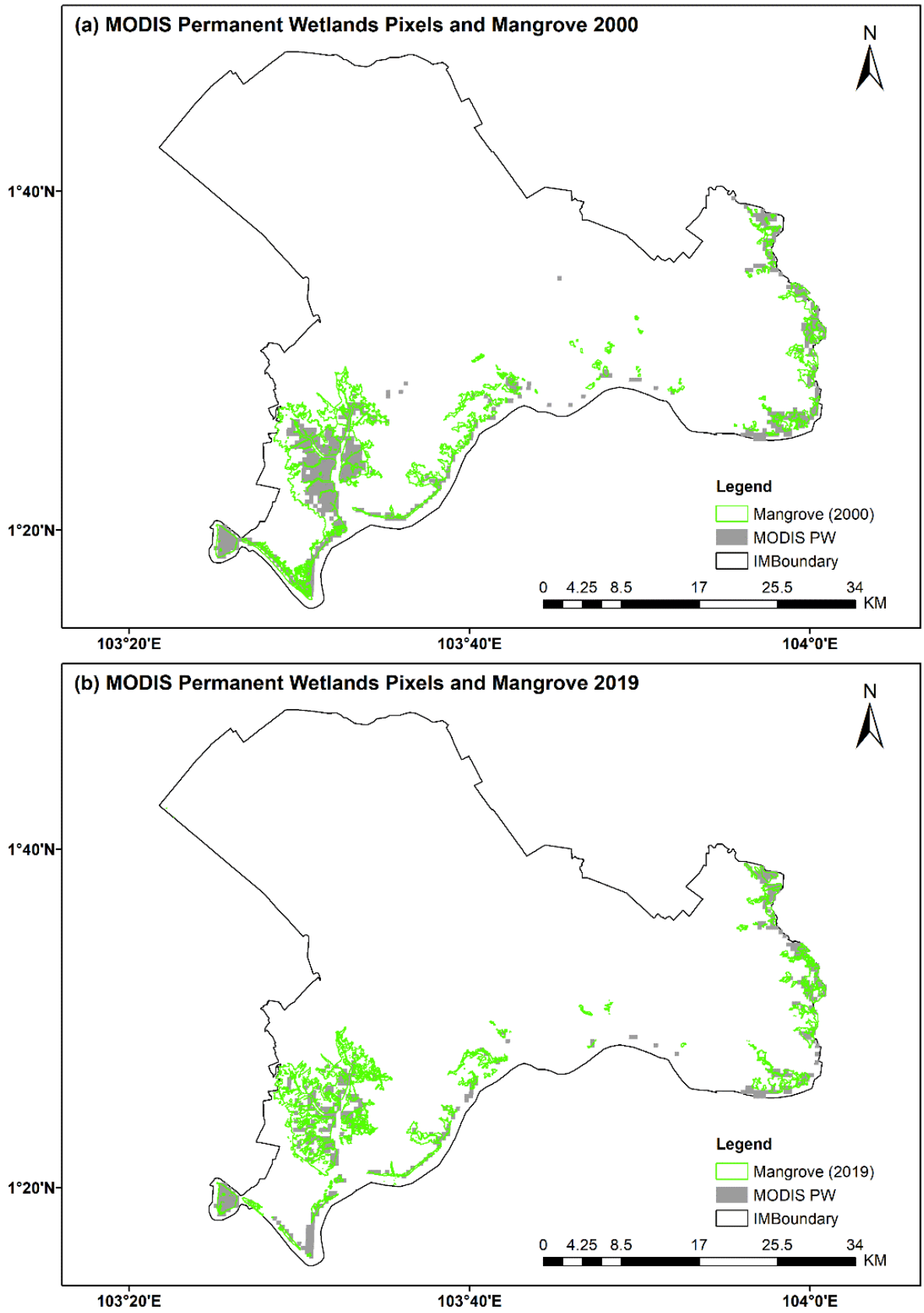

Figure 5. Mangrove area overlaid with the MODIS Permanent Wetlands pixels for year (**a**) 2000 and (**b**) year 2019.

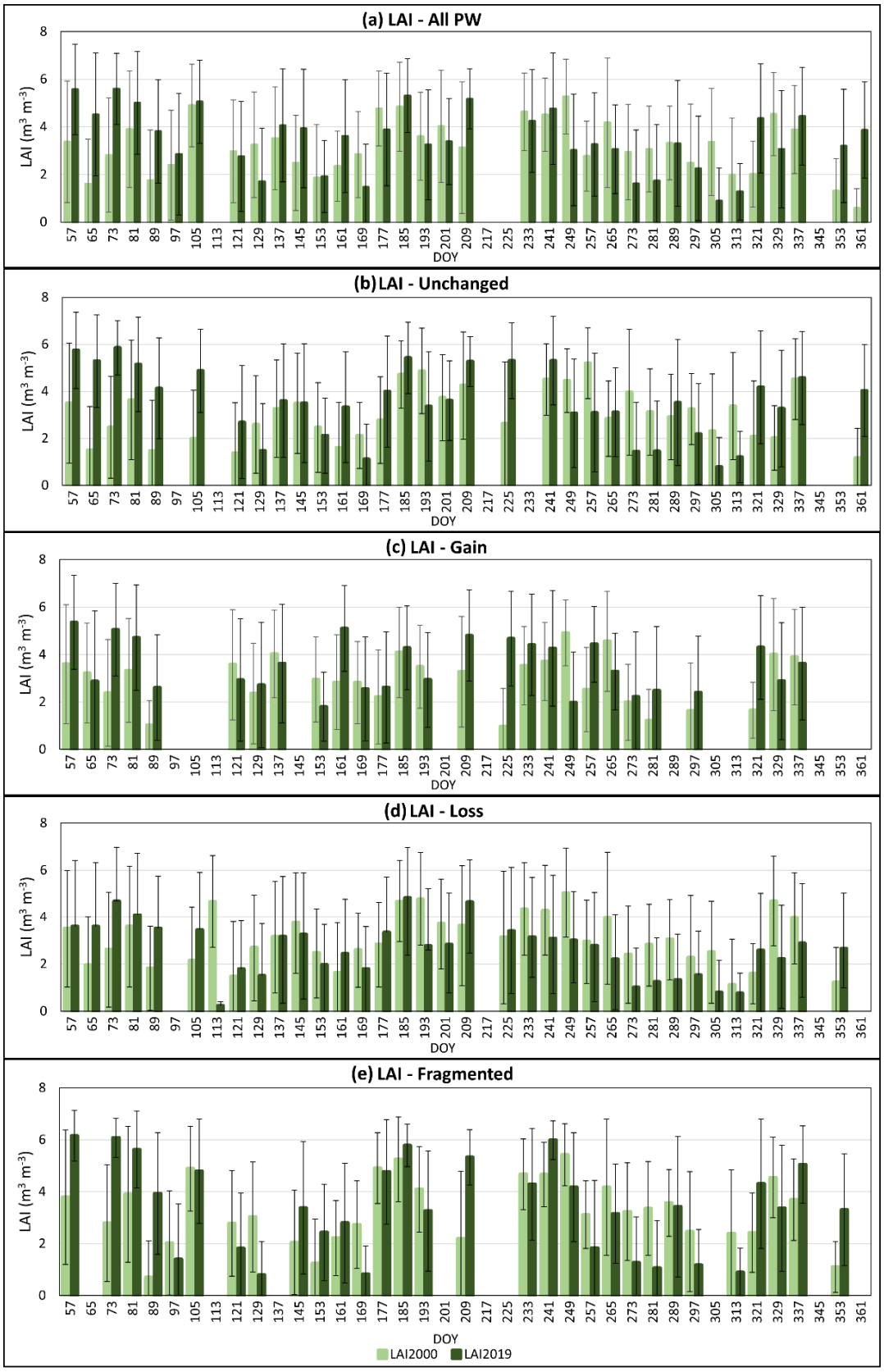

Figure 6. MODIS LAI values extracted based on (**a**) all mangrove area, (**b**) mangrove no change area, (**c**) mangrove gain area, (**d**) mangrove loss area, and (**e**) fragmented mangrove area.

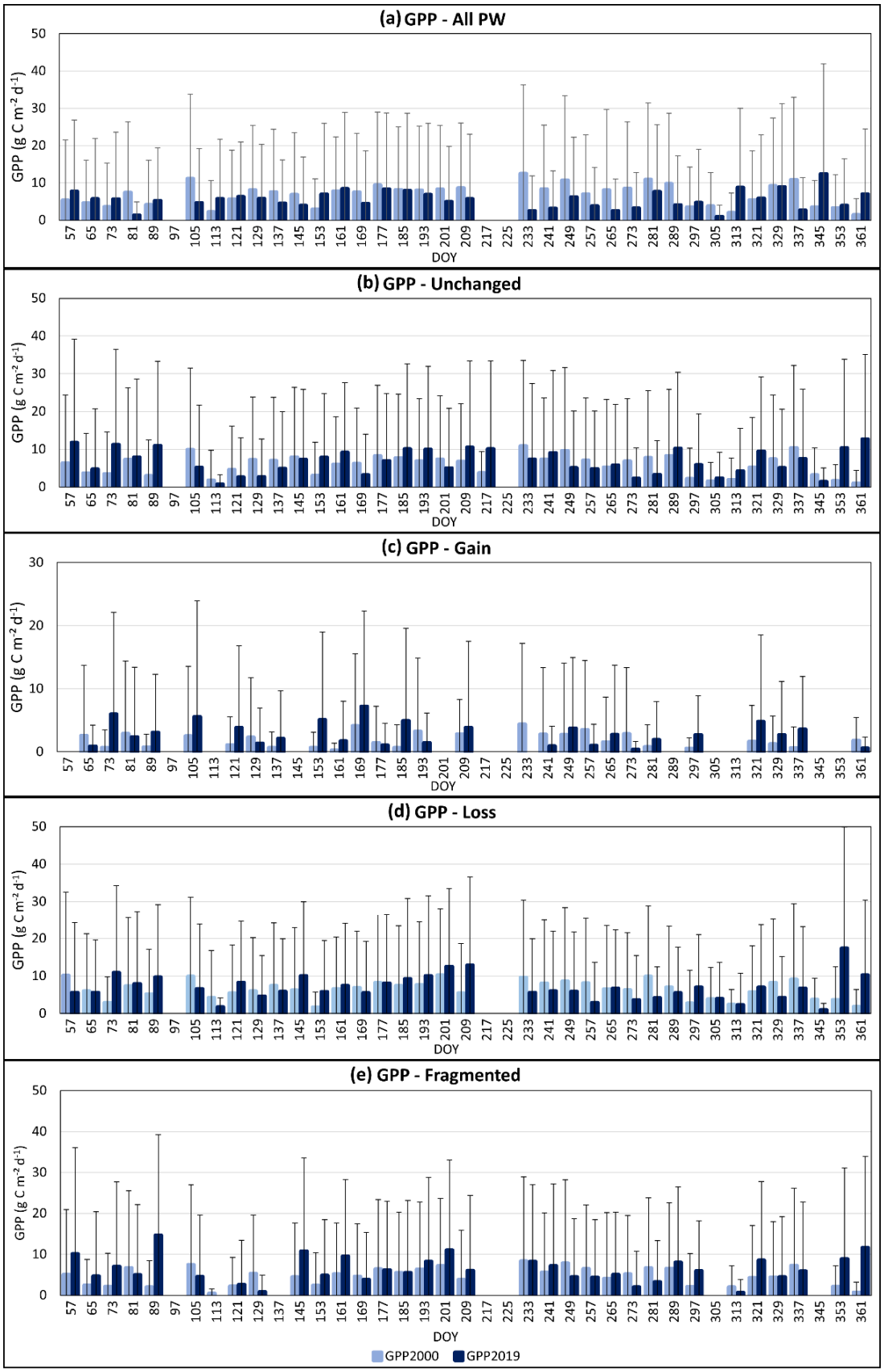

Figure 7. MODIS GPP values extracted based on (**a**) all mangrove area, (**b**) mangrove no change area, (**c**) mangrove gain area, (**d**) mangrove loss area, and (**e**) fragmented mangrove area.

Figure 6a shows the mean LAI extracted from the MODIS 8-day product overlaid with all of the PW pixels found in the classified mangrove area. The yearly mean LAI was 3.18 ± 1.56 (mean ± standard deviation) with minimum and maximum values of 0.10 and 6.90, respectively, for the year 2000; while it was 3.46 ± 2.09 (mean ± standard deviation) with minimum of 0.10 and maximum of 6.60 for the year 2019. Figure 6b shows that the values extracted from the PW pixels on the unchanged mangrove area also showed an increasing trend, increasing from 3.03 to 3.55 for the years 2000 and 2019, respectively. The increases of mean LAI for all PW and unchanged areas indicate that the mangrove leaf area has grown over the years. Previous analysis (Section 3.1 and Figure 3c) show that relatively less mangrove gain was noticed when compared to area of mangrove loss. Based on the values in Figure 6c,d, the mean LAI extracted from the mangrove gain increased from 2.81 to 3.51, while the mangrove loss area recorded mean LAI decrease from 2.99 to 2.62, respectively. The loss of native mangrove trees, which have dense leaves, to oil palm, which have a less dense canopy, may be the main reason for the reduced LAI values. The mean LAI values were found to correspond to the growth or loss of the mangrove in the study area. Note that the standard deviation values of the LAI are relatively high, which might be due to the changes in LAI values but are also dependent on species composition, forest structure, and vegetative phenology, which are all intrinsically related to temperature and rainfall, and this may need to be examined further.

GPP serves as one of the most important parameters in global carbon analysis, ecosystem assessment, and monitoring of environmental changes [56,57]. To date, studies relating to mangrove ecosystem processes (including Net Primary Production) have been few, and the majority of them depend on ground-based flux data (i.e., FLUXNET), which are restricted to certain locations [21,58,59]. Introducing remote sensing products such as MODIS GPP could be a solution that will help in improving and extending the study of mangrove carbon processes at a larger scale. Figure 7 shows the GPP values extracted in this study based on the five cases. For all PW pixels (Figure 7a), a reduction in mean GPP from 6.82 g C m^{-2} to 5.49 g C m^{-2} is noticed. This reduction could be due to the lower GPP contributions by the newly gained mangroves in the PW pixels, which may have lowered the productivity of the whole area. Figure 7b shows the GPP values of the area with no change. The mean GPP of these pixels increased from 5.81 g C m^{-2} to 6.73 g C m^{-2}. The increase of mean GPP over the no change area shows the great ability of mangrove forests to assimilate CO_2. Over the mangrove gain areas, the mean GPP shows an increasing trend from 1.88 g C m^{-2} to 2.78 g C m^{-2}. Most of the mangrove gained areas were found to be mangroves regrown from abandoned aquaculture ponds. Recent studies [60,61] confirmed that the regrowth of the *Rhizophoraceae* family on the abandoned ponds is feasible, thus supporting the increase of GPP over the gained areas. For the mangrove loss area, mean GPP increased only slightly from 6.38 g C m^{-2} to 6.68 g C m^{-2}. Based on the classification results, most of the mangrove losses are due to transformation of the mangrove areas to oil palm cultivation. The fast-growing oil palm cultivation surrounding the mangrove areas, which are mixed in the larger MODIS pixels (500m), could be the reason for increasing GPP despite the loss of mangrove.

The effect of fragmentation on CO_2 assimilation and biomass accumulation by ecosystems is dependent on the size and location of the fragmented patches [62]. To analyze the impact of mangrove fragmentation on the LAI and GPP, we selected the patch of mangrove area with the largest loss (6883.06 ha in 2000), with a loss 1131.68 ha (16.54%) of mangroves and which had fragmented into 60 smaller patches between 2019 and 2000. The mean LAI and GPP values extracted from the MODIS products (Figures 6e and 7e) show a slight increase from 3.11 to 3.41 and a large change from 4.65 g C m^{-2} to 6.37 g C m^{-2}, respectively. Of the fragmented patches, six are of a very large size—total of 5704.50 ha (82.88% of the total area) compared to the MPS (26.63—Table 6), one patch is 17.27 ha, and the remaining 53 patches are smaller than 9 ha. According to Laurance et al. [63], the interior of relatively large fragments tends to change less following fragmentation than it does at the forest margins. This may be due to the edge effects, such as altered microclimate, which

do not penetrate into the core habitat of the forest interior. Peh, Lin, Luke, Foster, and Turner [18] concluded that productivity is stable in fragments of more than 9 ha. Therefore, despite serious fragmentation over this selected patch, the increases of LAI and GPP may be supported by the impact of fragmentation on productivity, and the survival rate of trees/plants may be higher in relatively smaller patches because the abundance of solar radiation along the edges of the patches may increase the productivity [63]. In smaller patches (<9 ha), the microclimate (temperature and rainfall) may also be changed, which may affect the productivity.

4. Discussion

4.1. Mangrove Classification and Loss

SVM classification has been widely explored on different types of remote sensing data and at global, regional, and local scales with high accuracy [64]. Mountrakis et al. [65] reviewed land cover classification using different techniques and concluded that SVM is superior compared to other classification techniques. Classification works related to mangrove area identification and mapping using SVM classifiers showed high accuracy [41,66,67]. SVM proved to be one of the best classifiers where high accuracy (~90%) was achieved based on the Landsat 7 ETM+ pan-sharpened image and the Sentinel-2A image. While several global mangrove maps are available at 30 m [34,53,68,69], the use of higher spatial resolution satellite images (15 m and 10 m) in this study aimed to increase the accuracy of mangrove extent mapping. The classification result showed clear delineation between mangrove, water bodies, and other land use and land cover, providing high quality mangrove cover in 2000 and 2019 for mangrove change identification. In a previous study, Kanniah, Sheikhi, Cracknell, Goh, Tan, Ho, and Rasli [32] performed land use classification of the IM region from 1989 to 2014 using multiple Landsat images. They showed that, during the 21st century, urban area significantly increased, converting from oil palm, rubber, mangrove, and forest.

The spatial pattern of mangrove changes in IM shows a significant loss in the southwestern part, where the three Ramsar sites are located (Figure 3c). The Ramsar sites have been protected since 2003; thus, the loss may be due to a high input of sediments generated via construction and land reclamation activities around the Sungai Pulai estuary [70], where the development of the Tanjung Bin Power Plant, the Forest City, and the expansion area of the Tanjung Pelepas Port (Figure 1) are located. Reports including the Marine Environment Protection Committee (MEPC) [71] stated that the increasing traffic of ships and vessels in this region generates wave currents that can destroy mangroves in coastal areas [72].

Within the mangrove region of IM, 40 sites with aquaculture activities were detected from the satellite images. Aquaculture conversion from mangrove forests is very popular, as can be seen in Indonesia, where there has been a 40% mangrove loss over the past three decades [73]. Figure 4b shows the locations of these aquaculture sites. Most of the aquaculture sites are located on the "others" land use, at the boundary of the mangrove area. Thus, we can conclude that aquaculture activities contributed greatly to the loss of mangrove areas during the study period. At the eastern side of IM (Figure 4b), more aquaculture sites were found compared to the western site (where the Ramsar sites are located). One of the reasons for this could be that the Ramsar sites are protected from these conversion activities while, on the eastern side, where the Johor River flows, the accessibility to water from the Johor River and the richness of nutrients at the site have encouraged the conversion of mangrove areas to aquaculture use.

4.2. Fragmentation

Based on all the fragmentation indices, the fragmentation of mangrove in the IM region indicates a serious impact on the ecosystem as the fragmented mangrove forests become ecologically and hydrologically isolated. A reduction of Class Area (CA) and Total Landscape Area (TLA) can decrease the movement zone of animals and discourage flora and fauna succession within or between fragments. An increased Number of Patches (NP)

and decreased mean patch size (MPS) mean that increasingly isolated mangrove patches lead to a loss of connectivity between patches, thus prolonging the migration of animals to surrounding habitats (due to the decreased existing habitat size or increased species diversity), which is one of the factors that stimulates species extinction [74]. The fragmentation analysis of the edge and shape indices reveal that human-induced disturbance is significantly influencing the mangrove forests. The decreased MSI value showed a reduction of shape complexity, which could be due to the transformation of mangrove areas (irregular shaped) into regularly shaped/spaced patches of urban, agricultural, and aquaculture uses. The changes of edge and shape complexity could ease human access to the fragmented patches and exploit the remaining mangrove forests. This could accelerate the loss and fragmentation of mangrove areas in the future. Fragmentation analysis can support decision-making on the conservation of mangrove area. The impact of fragmentation to the mangrove ecosystem should be the focus of future study. Identification of the vulnerable mangrove patches and/or areas for immediate actions and further regrowth/preservation plans must be implemented to ensure the longevity of mangrove forests in the IM, as well as in Malaysia as a whole.

4.3. Mangrove LAI and GPP

The measurement of leaf area and biomass of mangrove at different scales (local, regional, and global) is very scarce. Traditional destructive methods require a high demand of manpower, cost, and time, and the allometric equations generated for biomass calculation are usually site specific [75]. The majority of the scientific data collection based on flux tower has only built on inland forests, and this kind of data is less available for wetland forests [76]. Therefore, we propose the initiative to relate MODIS LAI and GPP to show their capability of detecting leaf area depletion and GPP rate changes of a selected area with active mangrove loss and fragmentation.

The LAI and GPP values extracted from MODIS products showed reliable values when compared to previous studies. Clough et al. [77] reported the LAI of the main mangrove species (*Rhizophora apiculata*) in Malaysia to be in the range of 3.10–5.10, which is within the range reported in IM (mean LAI from All PW pixels, 3.18–3.46, respectively in 2000 and 2019). In another study, Shrestha et al. [78] showed MODIS GPP to have a good match with the modelled GPP of a mangrove area in India, which can be useful for carbon assimilation estimation. The mean GPP of mangroves in the IM region is 5.49 g C m^{-2} (based on 2019 data), and this value is close to the GPP value of the tropical forests in Asia and the Americas, which are in the range of 8.22 and 10.96 g C m^{-2}. Nevertheless, it should be noted that the sparse resolution of MODIS products (500 m) could have a mixing pixel issue, where the contribution of oil palm plantation can affect the accuracy of the LAI and GPP. Thus, data with higher spatial resolution can improve future analysis.

Mangrove forests serve multiple functions that are significant in terms of ecology and economy, and these functions will be lost or reduced due to mangrove fragmentation. The unique forms and rich biodiversity of mangrove forests can provide tourism and recreational activities, including wildlife-watching and fishing [79]. Mangrove forests can be transformed as habitats and nursery grounds for a variety of flora and fauna [57,80], while mangrove trees are also functional as a source of food, fuel, and building materials [81]. Mangrove forests are also effective at protecting shorelines, thus preventing soil erosion, shoreline depletion, and floods [82]. Recent studies have revealed the potential of mangrove ecosystems in sequestrating CO_2 from the atmosphere, thereby reducing the impact of global warming and climate change [21,83]. The complex structure of mangroves with trunk, branches, leaves, various types of roots, and soil enable the ecosystem to store a high volume of carbon (450 Mg ha^{-1}) [83]. Mangrove forests have an equal global averaged biomass (247 t ha^{-1}) to humid evergreen tropical forests [57,84]. Significant deforestation and degradation of mangrove forests also leads to the loss of a relatively large carbon pool [9,85].

5. Conclusions

Mangrove forest loss has become a significant environmental issue over the past few decades, mainly due to the disruption of their ecosystem functions and services. Although various mangrove conservation and preservation actions have been initiated worldwide, mangrove losses and fragmentation are still ongoing in order to fulfil the insatiable needs of human beings. In Iskandar Malaysia, mass development has been ongoing and has destroyed the mangrove cover and fragmented the landscape. Such changes have been shown in this study to affect the areal extent of mangroves, their leaf area, and thereby the potential of the ecosystem to assimilate and accumulate carbon dioxide from the atmosphere. In the last two decades, a net loss of 2907 ha of mangrove has been estimated in this study using freely available medium-high resolution remote sensing data. It is noteworthy that the annual loss rate of 1.12%, is higher than the world's mangrove loss rate, and the study identified urbanization, oil palm plantations, and aquaculture activities as the main reasons for the land conversions in this region. Land cover changes of mangroves involved a reduction in the mean patch size from 105 ha to 27 ha and an increase in the number of mangrove patches from 130 to 402. Other fragmentation indices, such as edge and shape complexity, also showed increased values. The impact of fragmentation on mangroves' primary productivity showed an increase of 37%, which could be related to the smaller patches (< 9 ha) that can allow more sunlight to penetrate the edges of the patches and hence increase the productivity. Thus, it can be concluded that the impact of fragmentation on mangrove productivity is also dependent on the fragmented patch characteristics. Despite most of the mangrove forests in IM being declared as Ramsar Sites, the land use change near these protected forests could aggravate other natural forms of destruction such as soil erosion and tidal changes, which could further affect small patches of mangroves. Nevertheless, the regrowth of mangrove trees has also been seen scattered over the IM region, which could be promoted in the immediate future. Accuracy in the monitoring of the LAI and GPP can assist in precision planting or rehabilitation of species and habitat. It can also be used as a powerful response tool for resource managers. This study introduced a novel approach, combining the mangrove classification results with fragmentation analysis and mangrove LAI and GPP data to reveal the impact of fragmentation on mangrove productivity in a region that hosts important mangrove (Ramsar) sites in Malaysia. Such results are expected to provide standard guidelines for a stronger policy formulation to protect the remaining mangroves in the region and in other mangrove areas. Further studies on how to prevent mangrove loss, how to reconnect the fragmented mangrove forests, and how to improve the carbon stock estimation to prove the value of mangrove to the ecosystem processes are equally important, now and in the future.

Author Contributions: Conceptualization, K.D.K.; formal analysis, K.D.K. and C.S.K.; data curation, K.D.K.; writing—original draft preparation, K.D.K. and C.S.K., writing—review and editing, K.D.K., C.S.K., S.S. and A.A.A.; supervision, K.D.K.; funding acquisition, K.D.K. All authors have read and agreed to the published version of the manuscript.

Funding: This research and the APC was funded by Universiti Teknologi Malaysia, grant numbers Q.J130000.2452.08G51, Q.J130000.3052.02M01, and Q.J130000.3052.02M11.

Institutional Review Board Statement: Not applicable.

Informed Consent Statement: Not applicable.

Data Availability Statement: The Landsat 7 ETM+ satellite image was downloaded from the GloVis website (https://glovis.usgs.gov/ (accessed on 15 March 2021)); the Sentinel-2A satellite image was downloaded from the Copernicus Open Access Hub (https://scihub.copernicus.eu/ (accessed on 15 March 2021)); and the MODIS LAI, GPP and Land cover type products were downloaded from the NASA Earthdata website (https://earthdata.nasa.gov/ (accessed on 15 March 2021)).

Acknowledgments: We acknowledge the Ministry of Education, Malaysia and Universiti Teknologi Malaysia (through research grants Q.J130000.2452.08G51, Q.J130000.3052.02M01, and Q.J130000.3052.02M11) for providing funding to conduct the study. We thank Nazarin Ezzaty and Fateen Nabilah for their help in downloading and processing the satellite data and the reviewers for their constructive comments and suggestions to improve the quality of this work.

Conflicts of Interest: The authors declare no conflict of interest.

Appendix A

Table A1. Characteristics of land cover types classified in the study area.

Land Cover Type	Characteristics
Forest	Primary and secondary forests area with high density of natural trees
Mangrove	Mangrove forests
Oil Palm	Oil palm trees at different ages
Rubber	Rubber trees
Urban	Urban area including residential, road networks, industrial and buildings
Water Bodies	Water surfaces including rivers and lakes
Others	Orchards, shrubs, bush, abandoned lands, aquaculture farms, etc.

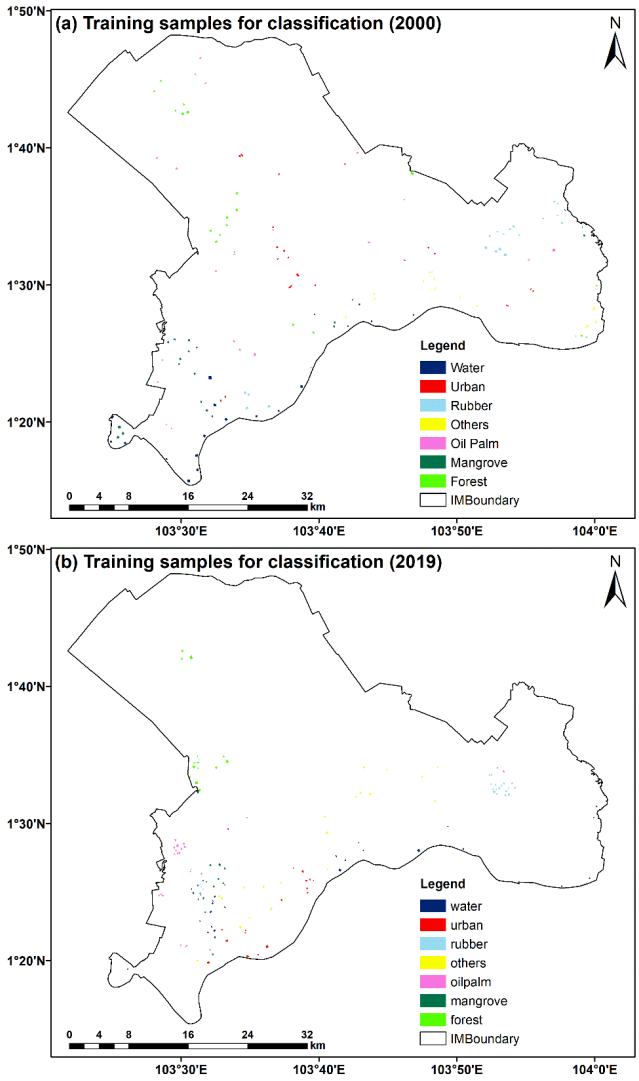

Figure A1. Training samples used for the SVM classification: (**a**) year 2000 and (**b**) year 2019.

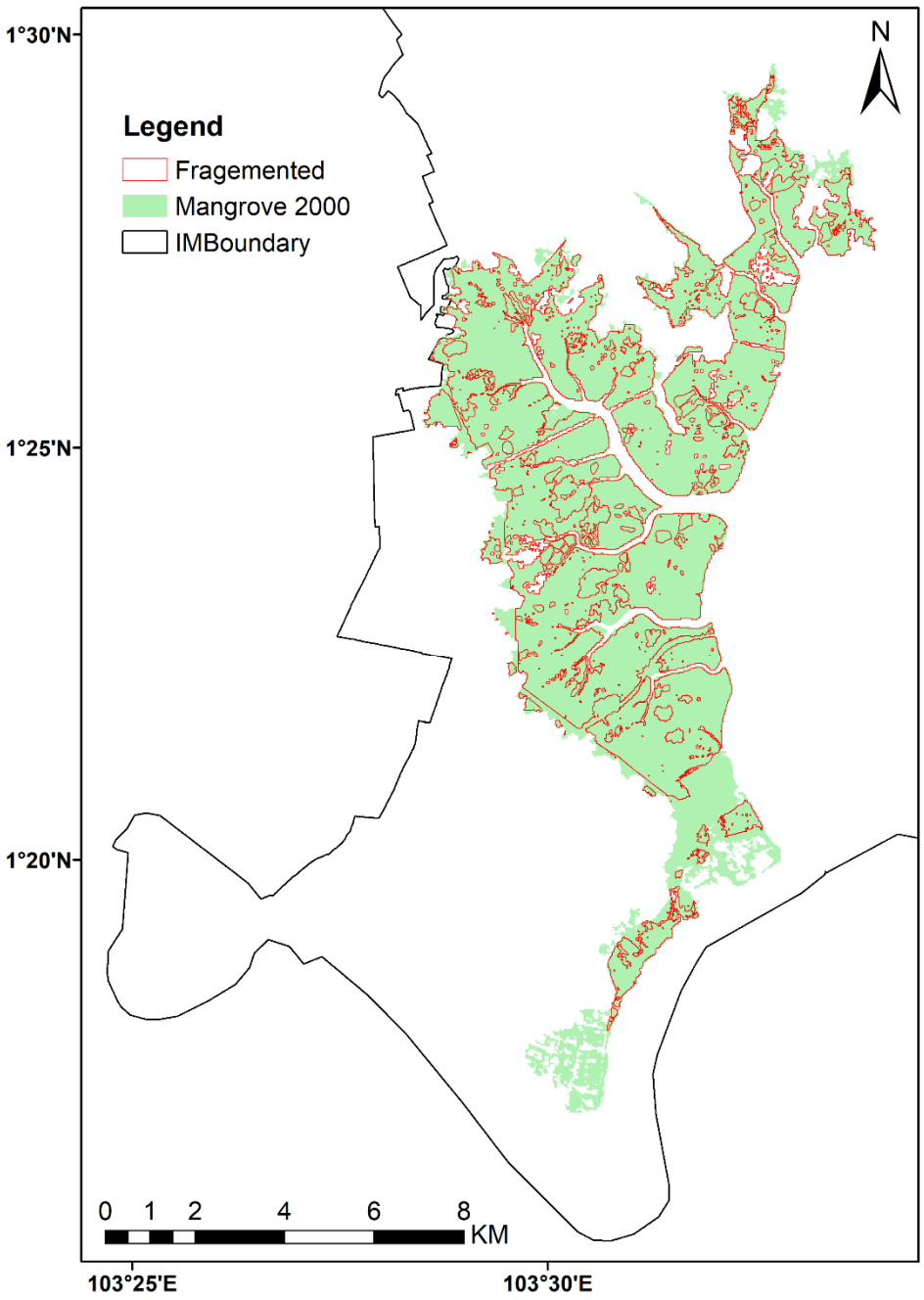

Figure A2. Selected area to show the fragmentation of the study area.

References

1. Bryan-Brown, D.N.; Connolly, R.M.; Richards, D.R.; Adame, F.; Friess, D.A.; Brown, C.J. Global trends in mangrove forest fragmentation. *Sci. Rep.* **2020**, *10*, 1–8. [CrossRef]
2. Herbeck, L.S.; Krumme, U.; Andersen, T.J.; Jennerjahn, T.C. Decadal trends in mangrove and pond aquaculture cover on Hainan (China) since 1966: Mangrove loss, fragmentation and associated biogeochemical changes. *Estuar. Coast. Shelf Sci.* **2020**, *233*, 106531. [CrossRef]
3. Ponnampalam, L.S.; Izmal, J.H.F.; Adulyanukosol, K.; Ooi, J.L.S.; Reynolds, J.E. Aligning conservation and research priorities for proactive species and habitat management: The case of dugongs Dugong dugon in Johor, Malaysia. *Oryx* **2014**, *49*, 743–749. [CrossRef]
4. Reyes-Arroyo, N.; Camacho-Valdez, V.; Saenz-Arroyo, A.; Infante-Mata, D. Socio-cultural analysis of ecosystem services provided by mangroves in La Encrucijada Biosphere Reserve, southeastern Mexico. *Local Environ.* **2021**, *26*, 86–109. [CrossRef]
5. Alemu, I.J.B.; Richards, D.R.; Gaw, L.Y.-F.; Masoudi, M.; Nathan, Y.; Friess, D.A. Identifying spatial patterns and interactions among multiple ecosystem services in an urban mangrove landscape. *Ecol. Indic.* **2021**, *121*, 107042. [CrossRef]

6. Seddon, N.; Daniels, E.; Davis, R.; Chausson, A.; Harris, R.; Hou-Jones, X.; Huq, S.; Kapos, V.; Mace, G.M.; Rizvi, A.R.; et al. Global recognition of the importance of nature-based solutions to the impacts of climate change. *Glob. Sustain.* **2020**, *3*, 1–12. [CrossRef]
7. Inácio, M.; Karnauskaitė, D.; Mikša, K.; Gomes, E.; Kalinauskas, M.; Pereira, P. *Nature-Based Solutions to Mitigate Coastal Floods and Associated Socioecological Impacts*; Metzler, J.B., Ed.; Springer: Berlin/Heidelberg, Germany, 2020; pp. 1–24.
8. Dahdouh-Guebas, F.; Ajonina, G.N.; Amir, A.A.; Andradi-Brown, D.A.; Aziz, I.; Balke, T.; Barbier, E.B.; Cannicci, S.; Cragg, S.M.; Cunha-Lignon, M.; et al. Public Perceptions of Mangrove Forests Matter for Their Conservation. *Front. Mar. Sci.* **2020**, *7*, 901. [CrossRef]
9. Sharma, S.; MacKenzie, R.A.; Tieng, T.; Soben, K.; Tulyasuwan, N.; Resanond, A.; Blate, G.; Litton, C.M. The impacts of degradation, deforestation and restoration on mangrove ecosystem carbon stocks across Cambodia. *Sci. Total. Environ.* **2020**, *706*, 135416. [CrossRef]
10. Sasmito, S.D.; Sillanpää, M.; Hayes, M.A.; Bachri, S.; Saragi-Sasmito, M.F.; Sidik, F.; Hanggara, B.B.; Mofu, W.Y.; Rumbiak, V.I.; Hendri; et al. Mangrove blue carbon stocks and dynamics are controlled by hydrogeomorphic settings and land-use change. *Glob. Chang. Biol.* **2020**, *26*, 3028–3039. [CrossRef]
11. Zeng, Y.; Friess, D.A.; Sarira, T.V.; Siman, K.; Koh, L.P. Global potential and limits of mangrove blue carbon for climate change mitigation. *Curr. Biol.* **2021**, in press. [CrossRef]
12. Sánchez-Núñez, D.A.; Pineda, J.E.M.; Osorio, A.F. From local-to global-scale control factors of wave attenuation in mangrove environments and the role of indirect mangrove wave attenuation. *Estuar. Coast. Shelf Sci.* **2020**, *245*, 106926. [CrossRef]
13. Kibler, K.M.; Kitsikoudis, V.; Donnelly, M.; Spiering, D.W.; Walters, L. Flow–Vegetation Interaction in a Living Shoreline Restoration and Potential Effect to Mangrove Recruitment. *Sustainability* **2019**, *11*, 3215. [CrossRef]
14. Friess, D.A.; Yando, E.S.; Abuchahla, G.M.; Adams, J.B.; Cannicci, S.; Canty, S.W.; Cavanaugh, K.C.; Connolly, R.M.; Cormier, N.; Dahdouh-Guebas, F.; et al. Mangroves give cause for conservation optimism, for now. *Curr. Biol.* **2020**, *30*, R153–R154. [CrossRef] [PubMed]
15. Worthington, T.A.; Andradi-Brown, D.A.; Bhargava, R.; Buelow, C.; Bunting, P.; Duncan, C.; Fatoyinbo, L.; Friess, D.A.; Goldberg, L.; Hilarides, L.; et al. Harnessing Big Data to Support the Conservation and Rehabilitation of Mangrove Forests Globally. *One Earth* **2020**, *2*, 429–443. [CrossRef]
16. Jacobson, A.P.; Riggio, J.; Tait, A.M.; Baillie, J.E.M. Global areas of low human impact ('Low Impact Areas') and fragmentation of the natural world. *Sci. Rep.* **2019**, *9*, 1–13. [CrossRef] [PubMed]
17. Rogan, J.E.; Lacher, T.E. Impacts of Habitat Loss and Fragmentation on Terrestrial Biodiversity. In *Reference Module in Earth Systems and Environmental Sciences*; Elsevier: Amsterdam, The Netherlands, 2018.
18. Peh, K.S.H.; Lin, Y.; Luke, S.H.; Foster, W.A.; Turner, E.C. Forest fragmentation and ecosystem function. *Glob. For. Fragm.* **2014**, 96–114. [CrossRef]
19. Chapin, F.S.; Woodwell, G.M.; Randerson, J.T.; Rastetter, E.B.; Lovett, G.M.; Baldocchi, D.D.; Clark, D.A.; Harmon, M.E.; Schimel, D.S.; Valentini, R.; et al. Reconciling Carbon-cycle Concepts, Terminology, and Methods. *Ecosystems* **2006**, *9*, 1041–1050. [CrossRef]
20. Braghiere, R.K.; Quaife, T.; Black, E.; He, L.; Chen, J.M. Underestimation of Global Photosynthesis in Earth System Models Due to Representation of Vegetation Structure. *Glob. Biogeochem. Cycles* **2019**, *33*, 1358–1369. [CrossRef]
21. Wang, L.; Jia, M.; Yin, D.; Tian, J. A review of remote sensing for mangrove forests: 1956–2018. *Remote Sens. Environ.* **2019**, *231*, 111223. [CrossRef]
22. Wicaksono, P.; Danoedoro, P.; Hartono; Nehren, U. Mangrove biomass carbon stock mapping of the Karimunjawa Islands using multispectral remote sensing. *Int. J. Remote Sens.* **2015**, *37*, 26–52. [CrossRef]
23. Hamdan, O.; Khairunnisa, M.; Ammar, A.; Hasmadi, I.M.; Aziz, H.K. Mangrove carbon stock assessment by optical satellite imagery. *J. Trop. For. Sci.* **2013**, *25*, 554–565.
24. Pham, T.D.; Yokoya, N.; Bui, D.T.; Yoshino, K.; Friess, D.A. Remote Sensing Approaches for Monitoring Mangrove Species, Structure, and Biomass: Opportunities and Challenges. *Remote Sens.* **2019**, *11*, 230. [CrossRef]
25. Pham, T.D.; Xia, J.; Ha, N.T.; Bui, D.T.; Le, N.N.; Tekeuchi, W. A Review of Remote Sensing Approaches for Monitoring Blue Carbon Ecosystems: Mangroves, Seagrassesand Salt Marshes during 2010–2018. *Sensors* **2019**, *19*, 1933. [CrossRef]
26. Running, S.; Mu, Q.; Zhao, M. MOD17A2H MODIS/Terra Gross Primary Productivity 8-Day L4 Global 500m SIN Grid VNASA EOSDIS Land Processes DAAC. 2015. Available online: https://doi.org/10.5067/MODIS/MOD17A2H.006 (accessed on 15 March 2021).
27. Patil, V.; Singh, A.; Naik, N.; Unnikrishnan, S. Estimation of Mangrove Carbon Stocks by Applying Remote Sensing and GIS Techniques. *Wetlands* **2015**, *35*, 695–707. [CrossRef]
28. Ishii, T.; Tateda, Y.; Ishil, T. Leaf area index and biomass estimation for mangrove plantation in Thailand. In Proceedings of the IGARSS 2004, 2004 IEEE International Geoscience and Remote Sensing Symposium, Anchorage, AK, USA, 20–24 September 2004; pp. 2323–2326.
29. Seto, K.C.; Fragkias, M. Mangrove conversion and aquaculture development in Vietnam: A remote sensing-based approach for evaluating the Ramsar Convention on Wetlands. *Glob. Environ. Chang.* **2007**, *17*, 486–500. [CrossRef]
30. Liu, D.; Li, S.; Fu, D.; Shen, C. Remote sensing analysis of mangrove distribution and dynamics in Zhanjiang from 1991 to 2011. *J. Oceanol. Limnol.* **2018**, *36*, 1597–1603. [CrossRef]

31. Shapiro, A.C.; Trettin, C.C.; Küchly, H.; Alavinapanah, S.; Bandeira, S. The Mangroves of the Zambezi Delta: Increase in Extent Observed via Satellite from 1994 to 2013. *Remote Sens.* **2015**, *7*, 16504–16518. [CrossRef]
32. Kanniah, K.D.; Sheikhi, A.; Cracknell, A.P.; Goh, H.C.; Tan, K.P.; Ho, C.S.; Rasli, F.N. Satellite Images for Monitoring Mangrove Cover Changes in a Fast Growing Economic Region in Southern Peninsular Malaysia. *Remote Sens.* **2015**, *7*, 14360–14385. [CrossRef]
33. De Alban, J.D.T.; Jamaludin, J.; De Wen, D.W.; Than, M.M.; Webb, E.L. Improved estimates of mangrove cover and change reveal catastrophic deforestation in Myanmar. *Environ. Res. Lett.* **2020**, *15*, 034034. [CrossRef]
34. Hansen, M.C.; Potapov, P.V.; Moore, R.; Hancher, M.; Turubanova, S.A.; Tyukavina, A.; Thau, D.; Stehman, S.V.; Goetz, S.J.; Loveland, T.R.; et al. High-Resolution Global Maps of 21st-Century Forest Cover Change. *Science* **2013**, *342*, 850–853. [CrossRef]
35. Kuenzer, C.; Bluemel, A.; Gebhardt, S.; Quoc, T.V.; Dech, S. Remote Sensing of Mangrove Ecosystems: A Review. *Remote Sens.* **2011**, *3*, 878–928. [CrossRef]
36. Omar, H.; Husin, T.M.; Parlan, I. *Status of Mangroves in Malaysia*; Forest Research Institute Malaysia: Selangor, Malaysia, 2020.
37. Friedl, M.; Sulla-Menashe, D. MCD12C1 MODIS/Terra+Aqua Land Cover Type Yearly L3 Global 0.05Deg CMG V006. NASA EOSDIS Land Processes DAAC. 2015. Available online: https://doi.org/10.5067/MODIS/MCD12C1.006 (accessed on 15 March 2021).
38. Myneni, R.; Knyazikhin, T.Y.; Park, T. MOD15A2H MODIS/Terra Leaf Area Index/FPAR 8-Day L4 Global 500m SIN Grid VNASA EOSDIS Land Processes DAAC. 2015. Available online: https://doi.org/10.5067/MODIS/MOD15A2H.006 (accessed on 15 March 2021).
39. Congedo, L. Semi-automatic classification plugin documentation. *Release* **2016**, *4*, 29.
40. Yuan, H.; Dai, Y.; Xiao, Z.; Ji, D.; Shangguan, W. Reprocessing the MODIS Leaf Area Index products for land surface and climate modelling. *Remote Sens. Environ.* **2011**, *115*, 1171–1187. [CrossRef]
41. Heumann, B.W. An Object-Based Classification of Mangroves Using a Hybrid Decision Tree—Support Vector Machine Approach. *Remote Sens.* **2011**, *3*, 2440–2460. [CrossRef]
42. Yu, L.; Gong, P. Google Earth as a virtual globe tool for Earth science applications at the global scale: Progress and perspectives. *Int. J. Remote Sens.* **2011**, *33*, 3966–3986. [CrossRef]
43. Dorais, A.; Cardille, J. Strategies for Incorporating High-Resolution Google Earth Databases to Guide and Validate Classifications: Understanding Deforestation in Borneo. *Remote Sens.* **2011**, *3*, 1157–1176. [CrossRef]
44. Kanniah, K.D. Quantifying green cover change for sustainable urban planning: A case of Kuala Lumpur, Malaysia. *Urban. For. Urban. Green.* **2017**, *27*, 287–304. [CrossRef]
45. Congalton, R.G.; Green, K. *Assessing the Accuracy of Remotely Sensed Data: Principles and Practices*; CRC Press: Boca Raton, FL, USA, 2019.
46. McGarigal, K. *FRAGSTATS: Spatial Pattern Analysis Program for Quantifying Landscape Structure*; US Forest Service Pacific Northwest Research Station: Portland, OR, USA, 1995; Volume 351.
47. Chen, J.M.; Ju, W.; Ciais, P.; Viovy, N.; Liu, R.; Liu, Y.; Lu, X. Vegetation structural change since 1981 significantly enhanced the terrestrial carbon sink. *Nat. Commun.* **2019**, *10*, 1–7. [CrossRef] [PubMed]
48. Li, Q.; Lu, X.; Wang, Y.; Huang, X.; Cox, P.M.; Luo, Y. Leaf area index identified as a major source of variability in modeled CO2 fertilization. *Biogeosciences* **2018**, *15*, 6909–6925. [CrossRef]
49. Vitale, L.; Di Tommasi, P.; D'Urso, G.; Magliulo, V. The response of ecosystem carbon fluxes to LAI and environmental drivers in a maize crop grown in two contrasting seasons. *Int. J. Biometeorol.* **2015**, *60*, 411–420. [CrossRef]
50. Amir, A.A.; Duke, N.C. Distinct characteristics of canopy gaps in the subtropical mangroves of Moreton Bay, Australia. *Estuar. Coast. Shelf Sci.* **2019**, *222*, 66–80. [CrossRef]
51. Kamal, M.; Phinn, S.; Johansen, K. Assessment of multi-resolution image data for mangrove leaf area index mapping. *Remote Sens. Environ.* **2016**, *176*, 242–254. [CrossRef]
52. Tian, Y.; Woodcock, C.E.; Wang, Y.; Privette, J.L.; Shabanov, N.V.; Zhou, L.; Zhang, Y.; Buermann, W.; Dong, J.; Veikkanen, B. Multiscale analysis and validation of the MODIS LAI productII. Sampling strategy. *Remote Sens. Environ.* **2002**, *83*, 431–441. [CrossRef]
53. Hamilton, S.E.; Casey, D. Creation of a high spatio-temporal resolution global database of continuous mangrove forest cover for the 21st century (CGMFC-21). *Glob. Ecol. Biogeogr.* **2016**, *25*, 729–738. [CrossRef]
54. Ewers, R.M.; Didham, R.K. The Effect of Fragment Shape and Species' Sensitivity to Habitat Edges on Animal Population Size. *Conserv. Biol.* **2007**, *21*, 926–936. [CrossRef] [PubMed]
55. Vaz, E. Managing urban coastal areas through landscape metrics: An assessment of Mumbai's mangrove system. *Ocean Coast. Manag.* **2014**, *98*, 27–37. [CrossRef]
56. Beer, C.; Reichstein, M.; Tomelleri, E.; Ciais, P.; Jung, M.; Carvalhais, N.; Rödenbeck, C.; Arain, M.A.; Baldocchi, D.; Bonan, G.B.; et al. Terrestrial gross carbon dioxide uptake: Global distribution and covariation with climate. *Science* **2010**, *329*, 834–838. [CrossRef] [PubMed]
57. Alongi, D.M. Carbon Cycling and Storage in Mangrove Forests. *Annu. Rev. Mar. Sci.* **2014**, *6*, 195–219. [CrossRef] [PubMed]
58. Gnanamoorthy, P.; Selvam, V.; Burman, P.K.D.; Chakraborty, S.; Karipot, A.; Nagarajan, R.; Ramasubramanian, R.; Song, Q.; Zhang, Y.; Grace, J. Seasonal variations of net ecosystem (CO_2) exchange in the Indian tropical mangrove forest of Pichavaram. *Estuar. Coast. Shelf Sci.* **2020**, *243*, 106828. [CrossRef]

59. Li, Q.; Lu, W.; Chen, H.; Luo, Y.; Lin, G. Differential Responses of Net Ecosystem Exchange of Carbon Dioxide to Light and Temperature between Spring and Neap Tides in Subtropical Mangrove Forests. *Sci. World J.* **2014**, *2014*, 1–11. [CrossRef]
60. Proisy, C.; Viennois, G.; Sidik, F.; Andayani, A.; Enright, J.A.; Guitet, S.; Gusmawati, N.; Lemonnier, H.; Muthusankar, G.; Olagoke, A.; et al. Monitoring mangrove forests after aquaculture abandonment using time series of very high spatial resolution satellite images: A case study from the Perancak estuary, Bali, Indonesia. *Mar. Pollut. Bull.* **2018**, *131*, 61–71. [CrossRef]
61. Bijsterveldt, C.E.J.V.; Wesenbeeck, B.V.; Wal, D.V.D.; Afiati, N.; Pribadi, R.; Brown, B.; Bouma, T. How to restore mangroves for greenbelt creation along eroding coasts with abandoned aquaculture ponds. *Estuar. Coast. Shelf Sci.* **2020**, *235*, 1–13. [CrossRef]
62. Collinge, S.K. Ecological consequences of habitat fragmentation: Implications for landscape architecture and planning. *Landsc. Urban. Plan.* **1996**, *36*, 59–77. [CrossRef]
63. Laurance, W.F.; Goosem, M.; Laurance, S.G. Impacts of roads and linear clearings on tropical forests. *Trends Ecol. Evol.* **2009**, *24*, 659–669. [CrossRef] [PubMed]
64. Sheykhmousa, M.; Mahdianpari, M.; Ghanbari, H.; Mohammadimanesh, F.; Ghamisi, P.; Homayouni, S. Support Vector Machine Versus Random Forest for Remote Sensing Image Classification: A Meta-Analysis and Systematic Review. *IEEE J. Sel. Top. Appl. Earth Obs. Remote Sens.* **2020**, *13*, 6308–6325. [CrossRef]
65. Mountrakis, G.; Im, J.; Ogole, C. Support vector machines in remote sensing: A review. *ISPRS J. Photogramm. Remote Sens.* **2011**, *66*, 247–259. [CrossRef]
66. Huang, X.; Zhang, L.; Wang, L. Evaluation of Morphological Texture Features for Mangrove Forest Mapping and Species Discrimination Using Multispectral IKONOS Imagery. *IEEE Geosci. Remote Sens. Lett.* **2009**, *6*, 393–397. [CrossRef]
67. Heumann, B.W. Satellite remote sensing of mangrove forests: Recent advances and future opportunities. *Prog. Phys. Geogr. Earth Environ.* **2011**, *35*, 87–108. [CrossRef]
68. Thomas, N.; Bunting, P.; Lucas, R.; Hardy, A.; Rosenqvist, A.; Fatoyinbo, T. Mapping Mangrove Extent and Change: A Globally Applicable Approach. *Remote Sens.* **2018**, *10*, 1466. [CrossRef]
69. Giri, C.; Ochieng, E.; Tieszen, L.L.; Zhu, Z.; Singh, A.; Loveland, T.; Masek, J.; Duke, N. Status and distribution of mangrove forests of the world using earth observation satellite data. *Glob. Ecol. Biogeogr.* **2011**, *20*, 154–159. [CrossRef]
70. Malaysia, S.A. *Impacts of Coastal Reclamation in Malaysia*; Sahabat Alam Malaysia: Penang, Malaysia, 2020.
71. MEPC. *Identification and Protection of Special Areas and Particularly Sensitive Sea Areas: Protection of Pulau Kukup (Kukup Island) and Tanjung Piai (Cape Piai)*; submitted by Malaysia, Singapore; Centre of International Law, National University of Singapore: Singapore, 28 April 2017.
72. McCreath, M. Burgeoning Practice of Southeast Asian States to Protect the Marine Environment from the Effects of International Shipping. *Asia-Pac. J. Ocean Law Policy* **2017**, *2*, 268–295. [CrossRef]
73. Murdiyarso, D.; Purbopuspito, J.; Kauffman, J.B.; Warren, M.W.; Sasmito, S.D.; Donato, D.C.; Manuri, S.; Krisnawati, H.; Taberima, S.; Kurnianto, S. The potential of Indonesian mangrove forests for global climate change mitigation. *Nat. Clim. Chang.* **2015**, *5*, 1089–1092. [CrossRef]
74. Haddad, N.M.; Brudvig, L.A.; Clobert, J.; Davies, K.F.; Gonzalez, A.; Holt, R.D.; Lovejoy, T.E.; Sexton, J.O.; Austin, M.P.; Collins, C.D.; et al. Habitat fragmentation and its lasting impact on Earth's ecosystems. *Sci. Adv.* **2015**, *1*, e1500052. [CrossRef] [PubMed]
75. Wang, D.; Wan, B.; Liu, J.; Su, Y.; Guo, Q.; Qiu, P.; Wu, X. Estimating aboveground biomass of the mangrove forests on northeast Hainan Island in China using an upscaling method from field plots, UAV-LiDAR data and Sentinel-2 imagery. *Int. J. Appl. Earth Obs. Geoinf.* **2020**, *85*, 101986. [CrossRef]
76. Rodda, S.R.; Thumaty, K.C.; Jha, C.S.; Dadhwal, V.K. Seasonal Variations of Carbon Dioxide, Water Vapor and Energy Fluxes in Tropical Indian Mangroves. *Forests* **2016**, *7*, 35. [CrossRef]
77. Clough, B.; Ong, J.; Gong, W. Estimating leaf area index and photosynthetic production in canopies of the mangrove Rhizophora apiculata. *Mar. Ecol. Prog. Ser.* **1997**, *159*, 285–292. [CrossRef]
78. Shrestha, S.; Miranda, I.; Kumar, A.; Pardo, M.L.E.; Dahal, S.; Rashid, T.; Remillard, C.; Mishra, D.R. Identifying and forecasting potential biophysical risk areas within a tropical mangrove ecosystem using multi-sensor data. *Int. J. Appl. Earth Obs. Geoinf.* **2019**, *74*, 281–294. [CrossRef]
79. Spalding, M.; Parrett, C.L. Global patterns in mangrove recreation and tourism. *Mar. Policy* **2019**, *110*, 103540. [CrossRef]
80. Glaser, M. Interrelations between mangrove ecosystem, local economy and social sustainability in Caeté Estuary, North Brazil. *Wetl. Ecol. Manag.* **2003**, *11*, 265–272. [CrossRef]
81. Giri, C.; Muhlhausen, J. Mangrove Forest Distributions and Dynamics in Madagascar (1975–2005). *Sensors* **2008**, *8*, 2104–2117. [CrossRef]
82. Das, S. Does mangrove plantation reduce coastal erosion? Assessment from the west coast of India. *Reg. Environ. Chang.* **2020**, *20*, 1–12. [CrossRef]
83. Ouyang, X.; Lee, S.Y. Improved estimates on global carbon stock and carbon pools in tidal wetlands. *Nat. Commun.* **2020**, *11*, 1–7. [CrossRef] [PubMed]
84. Kanniah, K.D.; Tan, K.P.; Cracknell, A.P.; Huete, A.R.; Idris, N.H.; Lau, A.M.S.; Rahman, M.Z.A.; Rasib, A.W.; Ahmad, A. Assessment of biophysical properties of Royal Belum tropical forest, Malaysia. *Singap. J. Trop. Geogr.* **2017**, *39*, 90–106. [CrossRef]
85. Richards, D.R.; Thompson, B.S.; Wijedasa, L. Quantifying net loss of global mangrove carbon stocks from 20 years of land cover change. *Nat. Commun.* **2020**, *11*, 1–7. [CrossRef] [PubMed]